Numerical analysis of the adhesive effect on moisture-induced stresses and deformations in CLT panels

by

Zahra Afshari

A Thesis Submitted in Partial Fulfillment of the Requirements for the Degree of

Master of Applied Science

in the Department of Civil Engineering

University of Victoria

Numerical analysis of the adhesive effect on moisture-induced stresses and deformations in CLT panels

by

Zahra Afshari

Supervisory Committee

Dr. Sardar Malek, Supervisor
Department of Civil Engineering

Dr. Phalguni Mukhopadhyaya, Academic Unit Member
Department of Civil Engineering

Dr. Min Sun, Academic Unit Member
Department of Civil Engineering

Abstract

Sustainable materials such as cross-laminated timbers (CLT) are increasingly being used in the construction of green buildings worldwide. Such products may be exposed to cyclic environmental conditions and exhibit moisture-induced damage. The main objective of this study is to develop and validate an efficient, physically-based tool to simulate the moisture transport, and consequently moisture-induced stresses and deformation in laminated orthotopic composites.

Predicting the moisture profile variation with time is the first step toward understanding the performance of CLT panels under extreme environmental loads. A comprehensive literature review was conducted to determine the most critical parameters in moisture transport phenomena in CLT panels to ensure the capability of the framework to capture the essential moisture transport mechanisms. Thermal moisture analogy theory was used for simulating the moisture transport across the composite material cross-section. Unlike previous studies, the moisture adsorption curve of the material was used instead of employing the surface emission coefficient to estimate moisture flux at the surfaces. The method was verified and validated based on a simple one-dimensional (1-D) analytical model and experimental data, respectively. A series of parametric studies were conducted using the validated model to highlight the effect of glue lines, wood species, boundary conditions, panel dimension, and orientation of CLT layers on the moisture transport across the composite panel.

After predicting the moisture profile of CLT panels, the numerical model was used to determine the stresses caused by humidity differences on panel surfaces. The applied transient load in the model was obtained from the moisture transport simulation. The total strain rate is assumed as the sum of the elastic and the moisture-induced strain rate. The mechano-sorptive strain is omitted from the material model since it is assumed that samples are not under mechanical loading. The stress model was successfully validated by experimental data reported in the literature. Parametric studies were conducted to investigate the significant role of panel bonding lines (i.e. elasticity modulus and moisture diffusivity) on moisture-induced stresses. A failure analysis was completed to determine how wood species affect laminated composite failure. The same approach was followed to determine the moisture-induced deformation through a finite element analysis. Finally, the effect of adhesive elasticity and its moisture diffusivity on the deformed shape of CLT panels was investigated parametrically. This study showed that the choice of adhesive along with the

combination of wood species, could significantly affect the panel's moisture profile and developed stresses even after 14 days under similar environmental conditions. As demonstrated in this thesis, simulating moisture transport in CLT panels is crucial in determining stresses and deformation caused by environmental conditions.

Table of Contents

List of Figures

List of Tables

Publications

Parts of the present thesis have been reported elsewhere as are listed below:

Journal

Z. Afshari, S. Malek, Moisture transport in laminated wood and bamboo composites bonded with thin adhesive layers–A numerical study, **Construction and Building Materials**. 340 (2022) 127597.

Conference

Z. Afshari, S. Malek, Numerical modeling of moisture transport in bamboo-based composite panels, **BIOCOMP2020, KOREA** (2021).

Acknowledgment

I have been fortunate to have had many individuals' support, guidance, and friendship throughout two years of my master's studies at the University of Victoria. This thesis is dedicated to all who have made this such as journey such an enjoyable learning process.

First and foremost, I would like to express my special appreciation and thanks to my supervisor Dr. Sardar Malek, who has been a tremendous mentor to me. I appreciate all his dedicated support and guidance support, both personally and professionally.

My sincere thanks to my committee members: Dr. Phalguni Mukhopadhyaya and Dr. Min Sun, for their time and constructive comments.

I gratefully acknowledge the University of Victoria for its financial and technical support.

Last but definitely not least, I must express my gratitude to my spouse for her continued support and encouragement. I was continually amazed by the patience of my dear sons, Nima and Noyan, who experienced all of the ups and downs of my research.

1 Introduction

1.1 Background

Wood, as a natural resource, is suitable for many types of building construction. Wood is renewable, biodegradable, recyclable, and stores carbon, resulting in a smaller environmental footprint than other building materials. The application of wood in timber structures has been developed for years. Fig 1.1 shows the history of using timber in construction. Cross Laminated Timber (CLT) panels are increasingly being used in the construction industry due to their higher structural capacity and dimensional stability compared to wood [1-2]. CLT is a prefabricated, solid-engineered wood panel. A CLT panel consists of several layers of lumber boards stacked in alternating directions and bonded with adhesives. CLT panels consist of an odd number of layers (three to seven layers). Applications for CLT include floors, walls, and roofs in buildings. The higher strength and dimensional stability of CLT panels make them cost-effective for multistory and long-span diaphragm applications. In structural systems, such as walls, floors, and roofs, CLT panels serve as load-bearing elements. In wall applications, the lumber used in the outer layers of a CLT panel is typically oriented vertically so its fibers run parallel to gravity loads, maximizing the wall's vertical load capacity [3]. In floor and roof applications, the lumber used in the outer layers is oriented parallel to the direction of the span.

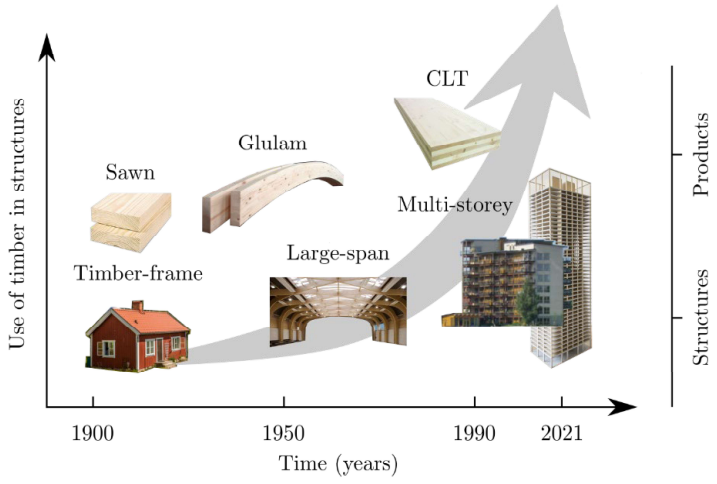

Fig 1.1: History of using timber in structures *[4]*

CLT panels continuously interact with their surrounding climate due to their hygroscopic properties. Wood absorbs moisture from the ambient air and swells when the environment's relative humidity (RH) increases. With a decrease in RH, such materials lose moisture and contract. From a mechanical perspective, permanent deformation or damage may occur if changes in RH and temperature are significant or frequent enough [5], [6]. Thus, the mechanical behavior and shape stability of CLT panels would be affected by changing the climate condition.

Researchers have found that moisture content variation is one of the main causes of timber damage [7]. Such damage commonly appeared as cracks in timber elements. Cracks would impact the performance of timber elements and are known as the primary damage type in timber elements, according to literature [7] (see Fig 1.2). Thus, predicting the moisture content is the first step toward understanding the performance of CLT panels under combined mechanical and environmental loads.

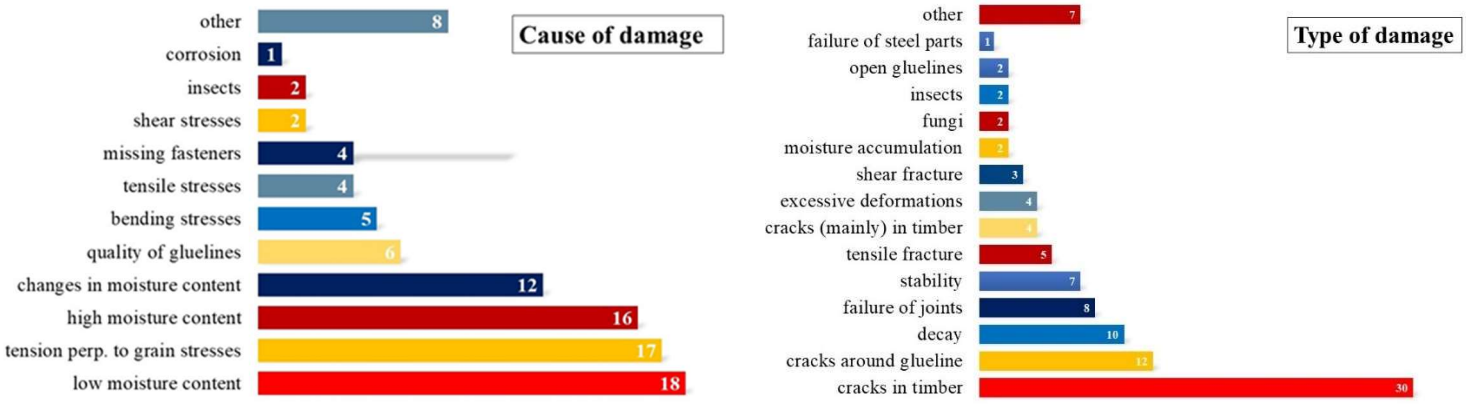

Fig 1.2: Evaluation of 245 assessments of large-span timber structures, left: cause of damage, right: type of damage *[7]*.

Several studies on simulating moisture diffusion into wood can be found in the literature. Simpson [8] investigated a mathematical relation between relative humidity and moisture content based on the sorption data of the U.S. Forest Products Laboratory [9]. Simpson [8] showed that the Hailwood and Horrobin models [10] provided the most accurate prediction of the maximum and minimum amount of moisture content in the outer regions of the panels. Franke et al. [11] developed a numerical model to estimate the influence of the climate on the wood moisture content and the risk to crack initiation in the long-span timber load-bearing elements. Sevenson et al. [12], Fortino et al. [13], and Autengruber et al. [14] conducted moisture simulations in timber elements.

They concluded that estimating moisture content in timber elements exposed to varying climates is critical for evaluating moisture-induced stresses in structural elements [12]–[18]. Although these studies have managed to estimate the moisture content in the selected timber elements, the effect of adhesives on the moisture profile of multi-layered timber elements has not been scrutinized.

Considering the significant effect of glue lines on the 3-D diffusion path is one of the challenges in modeling the moisture diffusion and predicting the moisture profile in CLT panels. This matter is of paramount importance when the physical properties, such as diffusion coefficient, change with the moisture content of the material at each point with time. As water diffuses through different wood layers, the glue lines may act as barriers and potential locations for moistening. This phenomenon could lead to local expansion/shrinkage at the glue lines, development of residual stresses, and ultimately debonding or splitting [19]–[21]. Hence, the presence of an adhesive layer and its physical properties should be considered for understanding the performance of engineered wood composites under extreme environmental loads and ultimately improving the durability of such composites.

1.2 Previous research on CLT panels

Unlike solid timber, studies on modeling moisture diffusion in cross-laminated timbers (and timber composite products in general) are quite rare. Several experimental studies were conducted to measure equilibrium moisture content and moisture diffusion in cross-laminated spruce panels using cup test [5], [22]–[24]. Results highlighted the effect of glue lines in laminated composite panels. The results from the cup test determined that the water vapor resistance of samples decreased with increasing voids between wood layers. Popper et al. [25] conducted cup tests to investigate the water vapor resistance of three and five-layered cross-laminated wood panels. The results showed that the water vapor resistance of selected panels is a function of glue lines' properties. Also, the study indicated the effect of glue line thickness per panel thickness ratio on the vapor resistance of laminated panels. The water vapor resistance increased with the increased glue lines per panel thickness. Furthermore, Popper et al. [25] reported a linear moisture diffusion pattern across the spruce panels. The complex set of experimental results led the researcher to complete numerical studies on moisture diffusion simulation in cross section of CLT panels.

Niemz et al. [26] studied the moisture diffusion in spruce CLT panels exposed to outdoor weathering. The moisture content was measured in 60 mm thick spruce panels in a climate of 90% RH at 20℃. Simulations showed good agreement with the measurements. Extending the work of Niemz et al. [26], Gereke [27] conducted a more comprehensive study on simulating moisture diffusion in three layered spruce panels when these panels were exposed to variable climate conditions (RH=65%-100%). The results confirmed the significant effect of glue lines on the moisture profile of spruce CLT. Gereke [27] employed mathematical equations to calculate the moisture diffusion coefficient of spruce and glue lines as a function of moisture content. His results showed that the selected values for the moisture diffusion coefficient of materials could significantly affect the moisture transfer across the CLT made of spruce layers bonded by one-component polyurethane (1K PUR) adhesive. However, the model of Gereke is only valid for the selected materials (spruce and 1K PUR) since the developed mathematical relation for diffusivity of materials were based on experiment.

In addition to moisture content measurements, Gereke [27]–[29] conducted experimental studies to measure moisture-induced deformation and moisture-induced stresses in CLT panels. Then a numerical model was developed to see the effect of CLT layers' thickness ratio and application of prestressed wood species on moisture-induced stress and deformation. Gereke [29] reported the highest deformation along the minor axis (*y-z* plane) in CLT panels. Also, it was shown that, with an increase in layer thickness ratio, the cup deformation increased, and stresses decreased. Using pre-stressed layers in the experiment showed significantly more minor moisture-induced deformation than the reference panel [29].

1.3 Objective

This research aims to complement the work of previous researchers by quantifying the adhesive effect on moisture-induced stresses in cross-laminated timber panels and proposing knowledge-based strategies to improve the dimensional stability of such panels. The primary goal is to find a general framework suitable for simulating CLT panels' moisture transport. Then, the moisture-induced stress and deformation are predicted by applying the simulated moisture transport to the model. Finally, through parametric studies, the influence of adhesive properties on the moisture-

induced response (stress and deformation) of CLT panels is determined. Strategies to reduce the developed stresses are discussed.

1.4 Thesis Outline

In this thesis, a finite element method has been developed and validated by previous experiments to investigate the effect of adhesive on moisture-induced stress and deformation of CLT panels. The outline of the thesis is as below:

In Chapter 2, numerical modeling is presented to simulate moisture transport in the cross-section of the CLT panel. After validation, several parametric studies are conducted to investigate the influence of adhesive types, wood species, boundary conditions, moisture exposure time duration, layers direction, and orthotropic moisture diffusivity on the moisture content of CLT layers.

In Chapter 3, simulation of moisture-induced stresses in CLT is described. After validation, the model is developed to select CLT panels with high and low moisture gradients at their glue lines. Then, failure analysis is performed on selected CLT panels to determine their moisture performance, and some parametric studies are conducted to explore the influence of adhesive properties (moisture diffusivity and elasticity) on CLT panels' moisture-induced stresses.

In Chapter 4, the described model in Chapter 3 is employed for simulating the moisture-induced deformation of CLT panels. Two parametric studies discuss the effect of adhesives on moisture-induced deformation.

1.5 Limitations

This study has the following limitations:

- The temperature is kept constant at T=20℃. Thus, the influence of temperature on moisture content and material properties has not been included in this thesis.
- A complete structure of CLT panels with several wooden planks in each layer was ignored in this study.
- The annual ring orientation is assumed constant, and different ring orientations are outside the scope of this study.

2 Moisture transport in CLT

2.1 Introduction

Wood is a porous material that absorbs moisture from the ambient air and swells when the environment's relative humidity (RH) increases. With a decrease in RH, wood loses moisture and contract. From a mechanical perspective, permanent deformation or damage may occur if changes in RH and temperature are significant or frequent enough [30], [31]. Modeling moisture transport in CLT panels is the first step in analyzing the stresses and deformations of these materials and their structural integrity under cyclic environmental loads.

One of the challenges in modeling the moisture transport and predicting the moisture profile in CLT panels is considering the significant effect of glue lines on the diffusion path. This is of paramount importance when the physical properties, such as diffusion coefficient, change with the moisture content of the material at each point with time. As water diffuses through different wood layers, the glue lines may act as barriers and potential locations for moistening [19], [26]. Hence, the presence of an adhesive layer and its thickness should be considered in modeling the moisture profile of CLT under the humidity gradient.

2.2 Definitions

This section defines the parameters considered for modeling moisture transport within the context of this thesis.

2.2.1 Equilibrium Moisture Content

Equilibrium moisture content definition (EMC) is the moisture level where the wood neither gains nor loses moisture since it is at equilibrium with the relative humidity and temperature of the surrounding environment [32]. This balance is crucial because wood continues to absorb and release moisture as the RH changes over time. To determine the EMC of the materials, moisture absorption isotherms are employed. Such isotherms are measured in a climate chamber with a constant temperature [27], [33]–[39]. The specimens are weighed when the mass is in equilibrium

with the chamber climate for various RH. Then, EMC can be reported when the two measurements differ less than 0.1%, according to the standard DIN 52183 [40].

For spruce, Gereke [27] conducted sorption measurements on $20mm \times 20mm \times 15mm$ wood specimens with a bulk density of $\rho_0 = 450\, kg/m^3$ at a constant temperature of 20℃ in a climate chamber. The measurements were performed at five relative humidity levels: 25%, 45%, 65%, 85%, and 93%. The results of such measurements were summarized in Fig 2.1. These results were used in determining moisture concentration (c) as the second parameter in simulating moisture diffusion profile in cross sections of laminated composite panels.

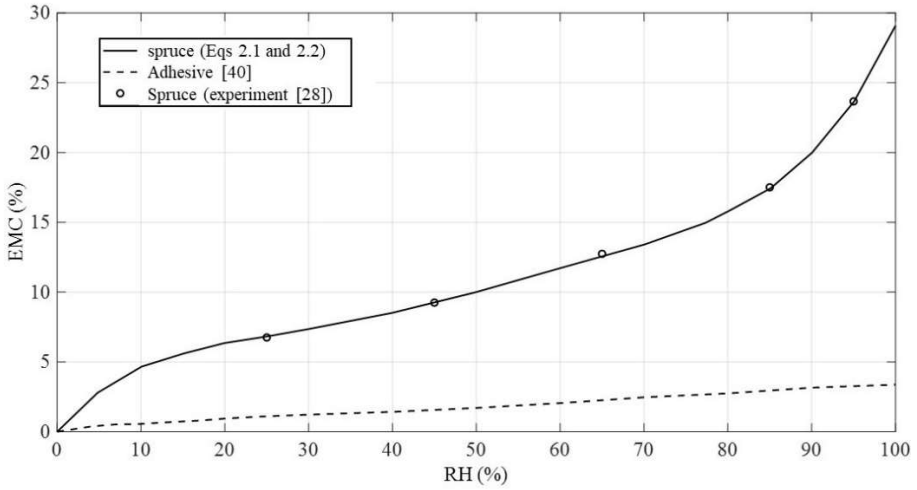

Fig 2.1: Sorption isotherm for spruce (solid line) and PUR adhesive (dashed line) at 20 ℃.

2.2.2 Moisture concentration

Moisture concentration (c), is defined as the amount of water per unit volume in wood and is an essential parameter in moisture transport studies. Knowing EMC, the c can be calculated using Eq 2.1.

$$c\ (kg/m^3) = EMC(\%).\frac{\rho_0}{100} \qquad \text{Eq 2.1}$$

For modeling purposes, a wide range of data for c values is needed. Therefore, sorption theories are applied to determine c. There are several theories to calculate c without performing experimental studies [8]. Siau and Simpson [8], [41] introduced a fifth-degree polynomial function (Eq 2.2) that gives the best fit to the experimental data.

$$c(\varphi, \rho_0) = 10(f_0 + f_1\varphi + f_2\rho_0 + f_3\varphi\rho_0 + f_4\varphi^2 + f_5\varphi^2\rho_0 + f_6\varphi^3 + f_7\varphi^3\rho_0 + f_8\varphi^4 + f_9\varphi^4\rho_0 + f_{10}\varphi^5 + f_{11}\varphi^5\rho_0) \quad \text{Eq 2.2}$$

where φ is the relative humidity (%) and ρ_0 is the bulk material density (kg/m^3). The coefficients (f_i) are fitting factors listed in Table 2.1 for spruce.

Table 2.1: Values of fi coefficients in the fifth-degree polynomial function for calculating moisture concentration (c) in spruce *[8], [41]*.

Coefficients	f_0	f_1	f_2	f_3	f_4	f_5
Value [-]	$-4.169.10^{-4}$	2.696	$-1.501.10^{-6}$	$6.714.10^{-2}$	-18.438	-0.294
Coefficients	f_6	f_7	f_8	f_9	f_{10}	f_{11}
Value [-]	45.036	0.715	-47.823	-0.797	18.515	0.338

Eq 2.2 does not need the EMC value to calculate the moisture concentration, c. Knowing the relative humidity and bulk density, the moisture concentration in the material can be estimated with Eq 2.1. It should be noted that this equation is only valid for spruce with oven-dry densities between 350 and 550 kg/m^3 [41]. Fig 2.2 shows a linear relationship between moisture concentration and oven-dry density of spruce.

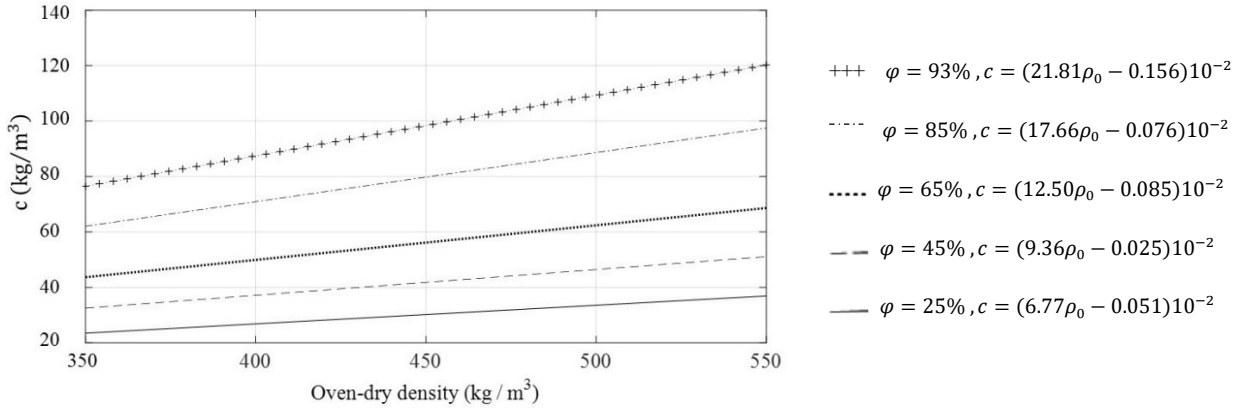

Fig 2.2: Linear relationship between moisture concentration (c) and density (ρ_0) of spruce at different relative humidity levels (φ) at constant T = 20°C. Results are generated using Eq 2.2 from reference *[41]*.

The moisture concentrations were calculated using Eq 2.2 for relative humidity levels ranging from 25% to 93%, considering an average density of $\rho_0 = 450\, kg/m^3$ for spruce. The moisture

concentration values were then converted into equilibrium moisture content values using Eq 2.1. The sorption isotherm of spruce obtained from Eq 2.1 is presented in Fig 2.1. An excellent fit with the data determined experimentally by Gereke [27] is noted. The sorption isotherm of the adhesive material (obtained separately from the literature [42]) was highlighted with a dashed line in Fig 2.1 for comparison purposes. It should be emphasized that the sorption isotherms showed very distinct behaviors, and the effect of adhesive layers may not be ignored.

2.2.3 Diffusion Coefficient

Diffusion of water refers to the molecular movement of bound water from a high water concentration region to a low one [43]. The rate at which water moves from one region to another passes through each unit of cross section per unit of time is termed moisture diffusion coefficient (D) [44]. The diffusion coefficient is a material property that may change with temperature and moisture content [8], [11], [19], [23], [45]–[47]. As it is noted in the literature, the diffusion coefficient of wood (D_w) strongly depends on the moisture content [27]. Fig 2.3 shows diffusion coefficient of spruce as a function of moisture content (MC), as applied in the present study. The relationship was plotted according to experimental studies of Siau [41].

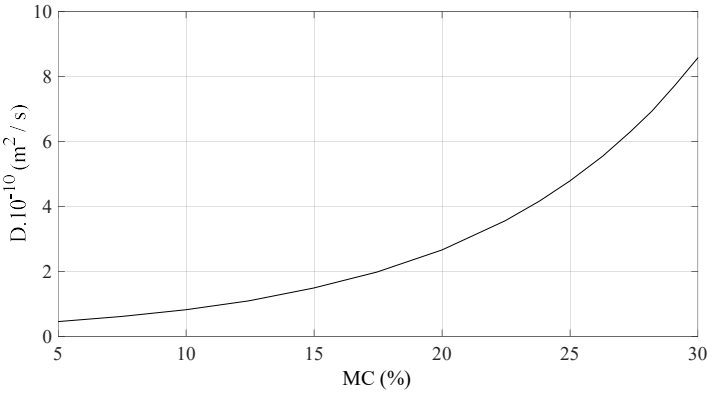

Fig 2.3: Variation of diffusion coefficient (D) of spruce with moisture content (MC) reported in Siau *[41]*.

In a separate study, Gereke investigated the relationship between the moisture diffusion coefficient (D) of spruce, moisture content (MC), and time (t) based on the experimental data [27]:

$$D_{(MC)} = 0.288e^{4(MC)} \qquad t > t^* \qquad [mm^2/h] \qquad \text{Eq 2.3}$$

$$D_{(MC,t)} = 0.288e^{4(MC)}\left(0.55\frac{t}{t^*} + 0.45\right) \quad t < t^* \qquad [mm^2/h]$$

where $t^* = 1000\ hours$.

It should be noted that the above relations (Eq 2.3) were concluded from the experimental measurements on spruce; hence they are only valid for spruce.

The information in experimental studies on the moisture diffusion coefficient of adhesives (D_{adh}) is very limited. Measuring the diffusion coefficient of adhesives is challenging since the adhesive foams during the chemical reaction with water [42]. Furthermore, as gluing techniques on layers of laminated composite panels require a mechanical process like pressuring, the diffusion coefficient for foamed adhesives (before being used in panels) will be significantly different from the values of *D* reported for adhesive materials that are used in the industry (not foamed adhesives) [42]. Wimmer et al. [42] conducted a comprehensive experimental study on moisture properties of various adhesives like PUR S309. The sorption isotherm of one-component foamed polyurethane was shown earlier in Fig 2.1. A value of $4.01 \times 10^{-12}\ m^2/s$ was selected for diffusion coefficient (D_{adh}) of the intended adhesive at T=20 ℃ and RH=65% based on Wimmer's [42] study. Some studies have assumed different values for D_{adh}. For example, Srpcic et al. [48] assumed $D_{adh} = D_{wood}$ and $D_{adh} = 0$ to determine the moisture profile of spruce CLT. The results showed that such assumptions do not correspond to the experimental results [27].

Gereke [27] showed that D_{adh} is a function of moisture concentration according to Eq 2.4 based on the experimental data.

$$D_{adh}(c) = \frac{A_1}{c^{A_2}} \times \rho_0 + A_3 \qquad \text{Eq 2.4}$$

where

$A_1 = 9.16 \times 10^{-13}\ \ [m^2/s]$

$A_2 = 0.51[-]$

$A_3 = -2.3 \times 10^{-12}\ [m^2/s]$

ρ_0 : Bulk density of adhesive $[kg/m^3]$

Fig 2.4 depicts the variation of D_{adh} with adhesive moisture concentration (c_{adh}) according to Eq 2.4.

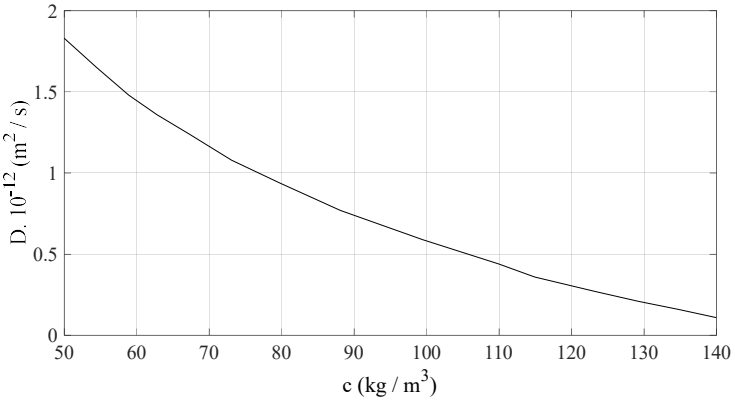

Fig 2.4: Variation of adhesive moisture diffusion coefficient (D) with the moisture concentration (c) based on experimental data and according to Eq 2.4 *[27]*.

Depending on the type of adhesive material being used, various values for MC in the middle layer of composite panels are expected based on the simulation. Therefore, accurate knowledge of the moisture behavior of adhesive bonds is crucial in simulating moisture diffusion through laminated composite panels.

2.3 Experiments

The result of an experimental study that was completed by Gereke [27] based on standard DIN EN ISO 12572 [49] has been used for validation purposes in this thesis. The examined specimen was a cylindrical three-layered spruce CLT bonded with PUR adhesive, and the thickness of each layer was 10 mm. Fig 2.5 shows the procedure of measuring MC in the CLT layers.

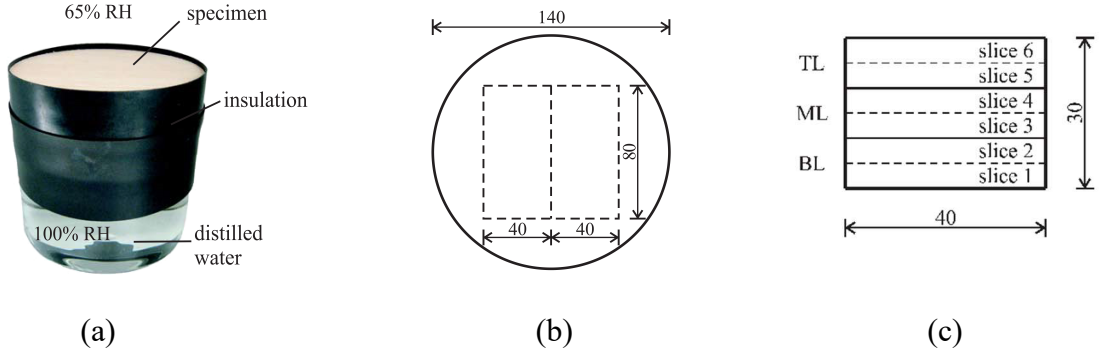

Fig 2.5: Procedure of the determination of moisture profiles, (a) test set-up, (b) cutting scheme in the cylindrical sample, (c) splitting into six layers [3].

In the first step, the specimen was conditioned at RH= 65% until moisture equilibrium was achieved. Then, the samples were fastened with rubber sleeves on cups filled with distilled water. The sleeves prevented the edge moisture sorption. A climate gradient of 65-100% RH was applied by placing the cups in a climate room. After 14, 21, 28, and 170 days, two rectangular samples with a dimension of $40mm \times 80mm$ were cut from the center of the specimen. Afterward, the layers were sliced to 5 mm thickness (see Fig 2.5). The MC of each 5 mm slice was determined by drying. The moisture content of layers' slices was reported as the MC of the outer and middle layers, according to Fig 2.6.

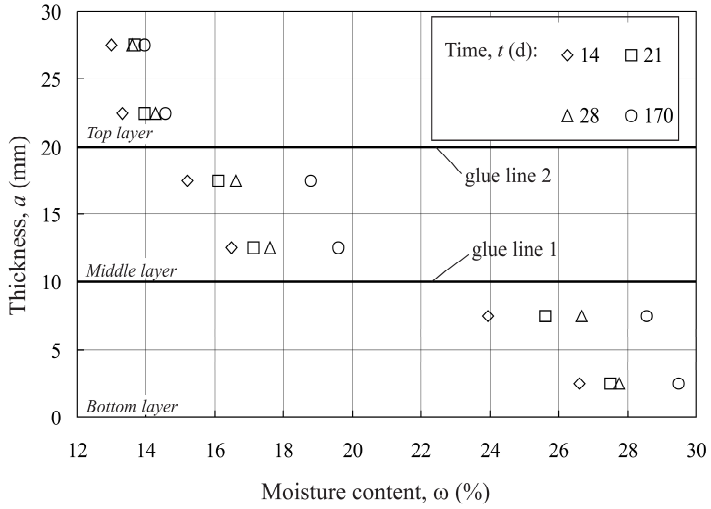

Fig 2.6: Measured moisture contents over the CLT panel thickness for 35% humidity difference *[27]*.

2.4 Numerical modeling

This section presents a modeling approach for simulating the moisture transport in the experimental study described in Section 2.3. The simulation results are compared with the testing data and numerical predictions of Gereke [40]. The developed model is then employed for various parametric studies in Section 2.5.

2.4.1 Material

According to Section 2.3, spruce and PUR are used as the wood and adhesive layers, respectively. Table 2.2 lists values for EMC (%), c (kg/m^3), and D (m^2/s) of these materials.

Table 2.2: Summary of Equilibrium Moisture Content (EMC), Moisture Concentration (c), and Moisture Diffusion Coefficient (D) values for spruce and PUR adhesive, at T=20 ℃ and RH=65%.

Material	Density (kg/m^3)	EMC (%)	$c_{100}{}^*$ (kg/m^3)	c_{65} (kg/m^3)	D (m^2/s)
spruce [27]	450	28.91	130.09	56.7	1.38×10^{-10}
adhesive (PUR S309) [42]	1000	3.36	33.6	22.2	4.01×10^{-12}

* c_{100} refers to moisture concentration at RH=100%

2.4.2 Method

To simulate moisture transport through layered composites, a multi-Fickian diffusion model [50] is adopted. For this purpose, the theory of thermal-moisture analogy is used to define materials' properties. After setting up thermal and moisture differential equations, the equivalent parameters of the moisture transfer equation (EMC, *c*, and *D*) were determined following the approach described in Section 2.4.2.1.

To assess the long-term effect of moisture exposure on moisture diffusion, the Transient Thermal solver of ANSYS was employed to estimate the moisture profile of the CLT panel. The purpose of a Transient Analysis is to determine the behavior of a model subjected to time-varying excitation. The moisture exchange between the ambient air and the surface of the model is described by Fick's first law, termed moisture flux, as Eq 2.5.

$$q = h(c_a - c_s) \quad \text{Eq 2.5}$$

where $c_a[kg/m^3]$ and c_s $[kg/m^3]$ are the equilibrium moisture concentration of the ambient air and wood surface, respectively. $q[kg/m^2s]$ is the moisture flux. *h* is a coefficient that represents the rate of moisture flux. There are several approaches to defining *h*. In previous studies, the moisture flux was estimated using the surface emission coefficient (e.g. [27], [41], [51], [52]) or film boundary coefficient (e.g. [14], [53]). However, determining the coefficient *h* is complex. Siau and Avramidis [51] believed that the theories to estimate the surface emission coefficient might not be applicable to dry hygroscopic materials such as wood at lower moisture content. In some other studies, the drying rate of the sample was used as the moisture flux (e.g. [54], [55]). The same function can be obtained from the moisture adsorption curve of materials [56]. Unlike previous studies, the moisture adsorption curve of the selected materials was used instead of

employing the surface emission coefficient to estimate moisture flux at the surfaces. Fig 2.7 displays the moisture adsorption curve of spruce for 35% humidity difference.

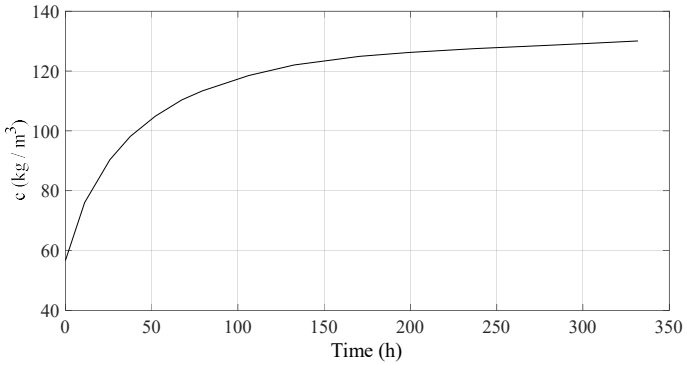

Fig 2.7: Moisture adsorption of spruce under the applied conditions (RH=65% to 100%) *[27]*.

Fig 2.8 displays the geometry and boundary condition of the model. A 65%-100% humidity difference for 14 days is applied to the model. The moisture concentration was calculated for the boundary conditions according to the thermal-moisture analogy (see Section 2.4.2.1). Moisture adsorption curves (obtained from the experimental studies) are employed as the moisture flux for 14 days of moisture exposure, based on Fig 2.7.

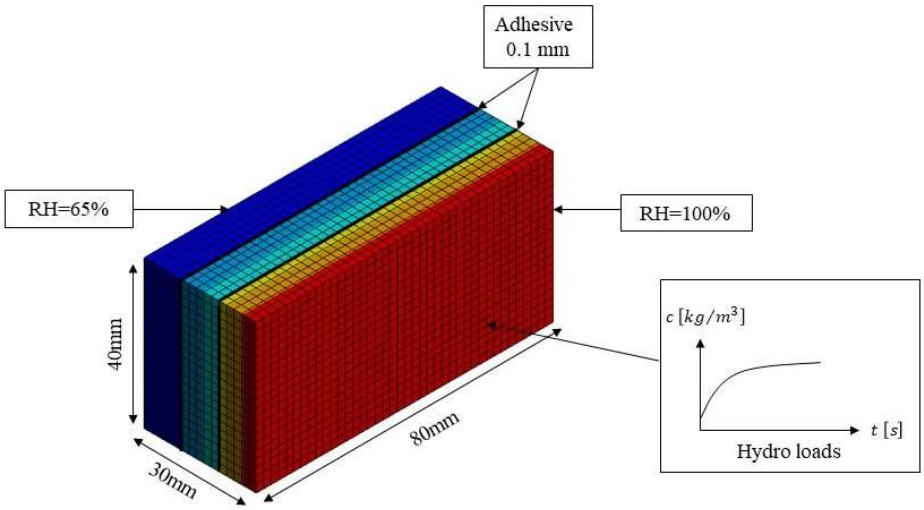

Fig 2.8: 3D model of three-layered composite panel bonded by two thin adhesive layers and the prescribed boundary condition.

2.4.2.1 Thermal moisture analogy

ANSYS Workbench© is used for the 3D modeling of moisture transfer in this thesis. Since ANSYS Mechanical solver does not offer mass transfer (e.g. moisture transfer), the thermal moisture analogy is required to simulate moisture transfer through ANSYS.

The conduction heat transfer can be described for isotropic materials by Fourier's law [57]:

$$q = -k \nabla T \quad \text{Eq 2.6}$$

where

T is temperature $[K]$,

q is heat flux $[Wm^{-2}]$,

∇ is the gradient operator,

k is the thermal conductivity $[Wm^{-1}K^{-1}]$.

In the case of no internal heat generation, the energy (thermal) balance leads to the governing equation for heat transfer as in Eq 3.14:

$$\rho C_p \frac{\partial T}{\partial t} + \nabla . q = 0 \quad \text{Eq 2.7}$$

where

ρ is the density $[kg\ m^{-3}]$,

C_p is the specific heat $[J\ kg^{-1}\ K^{-1}]$.

Assuming that thermal conductivity is uniform (i.e. $\nabla k = 0$), combining Eq 2.6 and Eq 2.7 results in the heat conduction equation (Eq 2.8):

$$\frac{\partial T}{\partial t} = \alpha \nabla^2 T \quad \text{Eq 2.8}$$

where

α is the thermal diffusivity $[m^2/s]$ defined as $\alpha = k/(\rho C_p)$.

Moisture diffusion can be described for isotropic materials by Fick's first law [50] according to Eq 2.9:

$$J = -D\,\nabla c \qquad \text{Eq 2.9}$$

where

J is the moisture flux $[kg/m^2 s]$;

c is the moisture concentration $[kg\ /m^3]$;

D is the moisture diffusion coefficient $[m^2/s]$.

In the case of no internal moisture generation, the governing equation of moisture diffusion becomes:

$$\frac{\partial c}{\partial t} + \nabla . J = 0 \qquad \text{Eq 2.10}$$

With an assumption of uniform moisture diffusion, combining Eq 2.9 and Eq 2.10 leads to the following moisture diffusion equation (Eq 2.11):

$$\frac{\partial c}{\partial t} = D\,\nabla^2\,c \qquad \text{Eq 2.11}$$

By inspecting the above equations, one can see that Fourier's mathematical expression (Eq 2.6) for heat conduction is very similar to Fick's second law (Eq 2.9). Hence, a diffusion problem can be analyzed using a typical heat transfer analysis in any finite element analysis (FEA) commercial software (e.g. ANSYS).

The comparison of Eq 2.8 and Eq 2.11 establishes the thermal-moisture analogy. A direct analogy between the two governing equations can be expressed as:

T (Temperature) ≡ ***c*** (Concentration)

α (Thermal diffusion coefficient) ≡ ***D*** (Moisture diffusion coefficient)

It should be noted that the analogy is written in the through-thickness direction of the material. The assumptions for deriving Eq 2.8 and Eq 2.11 were based on utilizing uniform conductivity and diffusivity. Consequently, this analogy is valid only when the thermal and moisture diffusivity is uniform within a hygroscopic material. This point implies that the hygroscopic material has to be homogeneous, and its temperature field must also be uniform at a given time [58].

The ambient temperature and relative humidity are assumed to be constant during the moisture exposure period (T= 20 ℃ and RH=65%). Moreover, materials are supposed to be homogenous (i.e. their conductivity and diffusivity are uniform across the materials). As a result, both assumptions for using the thermal-moisture analogy have been satisfied. Table 2.3 describes the parameters used in the thermal-moisture analogy employed in this thesis.

Table 2.3: FEA Thermal-Moisture Analogy parameters [56].

Thermal Analysis	Moisture Analysis
Field Variable (Temperature)	Field Variable (Water Concentration)
Density (ρ $[kg\ /m^3]$)	Density (1 $[kg\ /m^3]$)
Conductivity (k $[W/mK]$)	$D \times c_{sat}[kg\ /m.s]$
Specific Heat Capacity ($C_p[J/kg.K]$)	$c_{sat}[kg/m^3]$

2.4.3 Results

The results of the numerical model developed in ANSYS© provide the estimated moisture profile of CLT panels considering their glue lines. The numerical simulation of MC in spruce CLT is shown in Fig 2.9. The result is in good agreement with the experiment and numerical studies completed by Gereke [27].

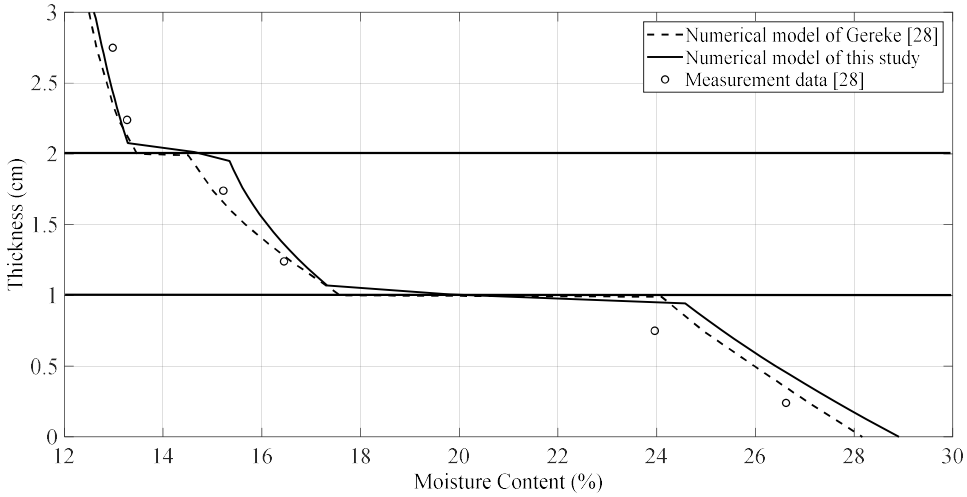

Fig 2.9: Moisture profile of spruce CLT panel obtained from numerical modeling and measurement data.

By comparing the simulation results with measurement data, it can be determined that using the moisture adsorption curve of the material as a boundary condition produces a moisture profile that is acceptable for transient analysis.

2.4.4 Verification

The simulations result from ANSYS were compared with 1-D analytical calculation using the heat transfer governing differential equations (Eq 2.8) to verify the applied analogy theory. Moisture concentration, $c(x,t)$, at each point (x) depends on the sample's thickness and moisture exposure time (t) based on the governing differential equation. A set of initial conditions (I.C) and boundary conditions (B.C) are required to solve the governing equation. Fig 2.10 illustrates the selected boundary conditions in the model. As in Gereke's experiments [27], the samples were placed at ambient with RH=65%, and the initial concentration was assumed to be $c = 56.7\ kg/m^3$ (i.e. RH=65%). The moisture concentration of spruce as a function of thickness (x) and time (t) can be determined by solving the equation below:

$$\frac{\partial T}{\partial t} = \alpha\, \nabla^2\, T \xrightarrow{thermal-moisture\ analogy} D.E:\ \alpha \frac{d^2c}{dx^2} - \frac{\partial c}{\partial t} = 0 \qquad \text{Eq 2.12}$$

where α is equal to:

$$\alpha = \frac{k}{\rho C_p} \qquad \text{Eq 2.13}$$

Considering $k, \rho\ and\ C_p$ from Table 2.3 for spruce, α becomes:

$$\alpha = \frac{1.79 \times 10^{-8}}{1 \times 130.09} = 1.38 \times 10^{-10}[m^2 s^{-1}] \qquad \text{Eq 2.14}$$

The initial and boundary conditions for solving Eq 2.12 is as below:

$$I.C\ :\ \{c_0 = c(x,0) = 56.7\ kg/m^3$$
$$B.C\ :\ \begin{cases} c(0,t) = 130.09\, kg/m^3 \\ c(0.03,t) = 56.7\, kg/m^3 \end{cases} \qquad \text{Eq 2.15}$$

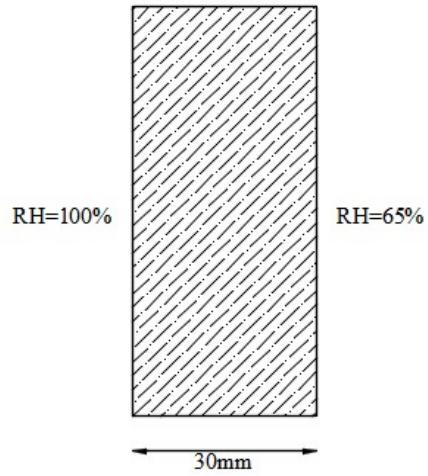

Fig 2.10: The boundary condition of the 1-D model considered for verification purposes.

The solution of Eq 2.8 can be written as:

$$c(x,t) = \sum_{n=1}^{\infty} B_n \sin(n\pi x) e^{-\alpha n^2 \pi^2 t} \qquad \text{Eq 2.16}$$

where

$$B_n = 2\int_0^1 \sin(n\pi x) f(x) dx \qquad \text{Eq 2.17}$$

and $f(x)$ is a function that shows the initial condition according to Eq 2.15. Replacing the initial condition according to Eq 2.15 in the Eq 2.17, results in B_n be equal to:

$$B_n = 2c_0 \int_0^1 \sin(n\pi x) dx \qquad \text{Eq 2.18}$$

Calculating the integrals in Eq 2.18 gives:

$$B_n = -2c_0 \frac{\cos(n\pi) - 1}{n\pi} = -\frac{2c_0}{n\pi}((-1)^n - 1) = \begin{cases} 0 & n \ \ even \\ \dfrac{4c_0}{n\pi} & n \quad odd \end{cases} \qquad \text{Eq 2.19}$$

In other words:

$$B_{2n} = 0 \quad , \quad B_{2n-1} = \frac{4c_0}{(2n-1)\pi} \qquad \text{Eq 2.20}$$

Hence, a solution can be obtained as:

$$c(x,t) = c_1 + (c_0 - c_1)\frac{4c_0}{\pi}\sum_{n=1}^{\infty}\frac{\sin(2n-1)\pi x}{(2n-1)}\exp\left(-\alpha(2n-1)^2\pi^2 t\right) \qquad \text{Eq 2.21}$$

where c_1 is the surface moisture concentration. For an exterior surface (x=0) exposed to RH=100%, $c_1 = c(0,t) = 130.09\,kg/m^3$ and for an interior surface (x=0.03 m) exposed to RH=65%, $c_1 = c(0.03,t) = 56.7\,kg/m^3$.

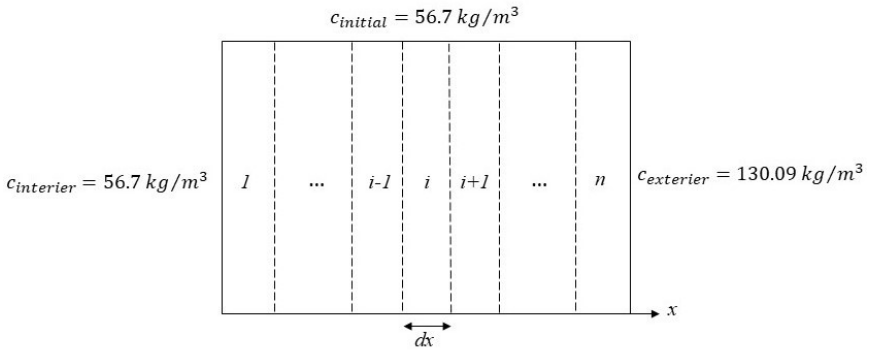

Fig 2.11: Schematic 1-D discretization in the analytical calculation of moisture diffusion problem.

MATLAB© software was used to perform the analytical calculations with Euler's method for 1 hour to 14 days of moisture exposure. Fig 2.11 shows the schematic discretization used in 1-D analytical approach. Comparing the analytical results with the numerical simulations in Fig 2.12 verifies the accuracy of the numerical model for moisture diffusion problems.

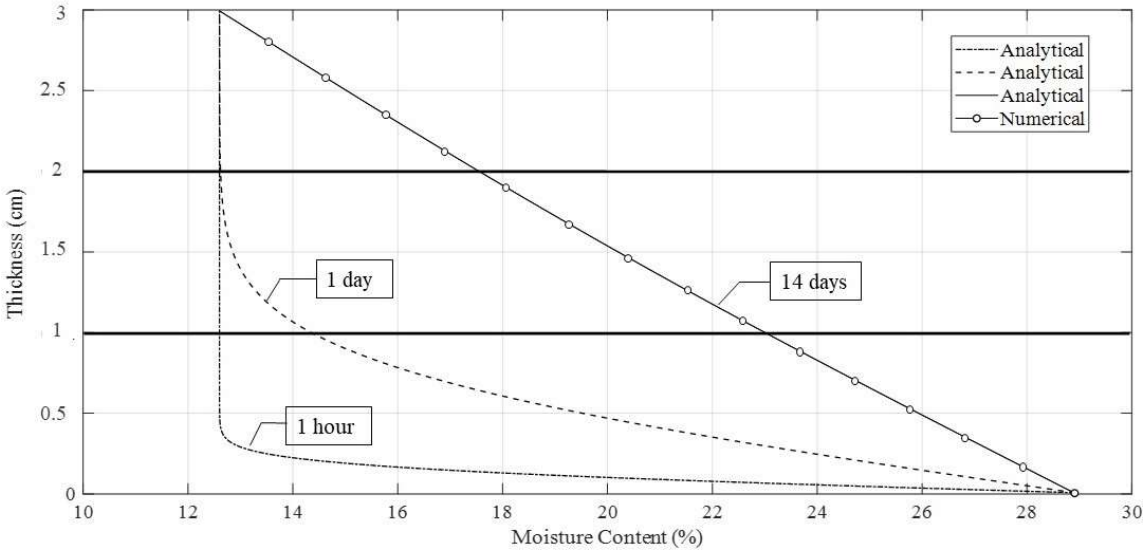

Fig 2.12: Moisture profile of spruce obtained from 1-D analytical calculation (lines) and numerical predictions (circles) for 14 days of moisture exposure.

2.4.5 Sensitivity analysis

A mesh sensitivity analysis was conducted with three different mesh sizes (see Table 2.4) to determine the correct element size for numerical results, and the results are presented in Fig 2.13. Based on the convergence study, Mesh 3 was selected for the case studies considered in the rest of this paper.

Table 2.4: Summary of the three different mesh sizes considered in the convergence study.

	Mesh 1	Mesh 2	Mesh 3
Number of elements	951	5121	12960
Number of nodes	160	1024	57173

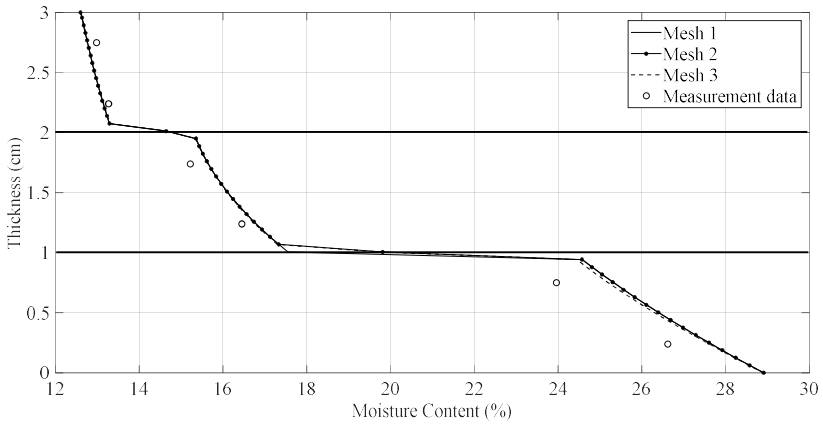

Fig 2.13: Moisture profile of spruce CLT panels after 14 days of moisture exposure using different mesh sizes: Panel is discretized with three mesh sizes (Mesh 1, Mesh 2, and Mesh 3) according to Table 2.4.

To determine the appropriate time step size in the FE analysis, the effect of the selected time step size on the predicted moisture profile is examined with Mesh 3. Three different time steps equal to 1000, 12096, and 120960 seconds are set in transient analysis of CLT panel exposed to moisture for 14 days (1209600 seconds). Fig 2.14 demonstrate that 1000 seconds is small enough to capture the converged moisture profile.

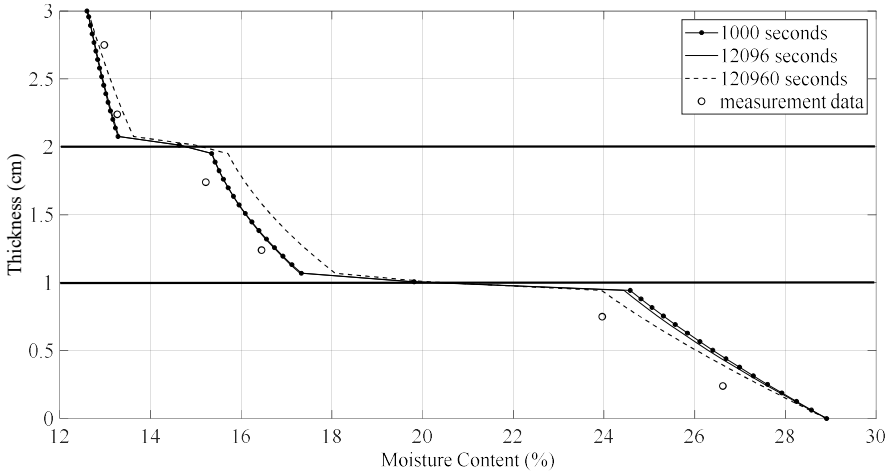

Fig 2.14: Moisture profile of spruce CLT panels after 14 days (or 1209600 seconds) moisture exposure using Mesh 3 with three different time step sizes: 1000, 12096, and 120960 seconds.

2.5 Parametric studies

The model was validated in Section 2.4.3. Thus, it can be employed to investigate the influence of different parameters on the moisture profile of CLT panels. Section 2.5.1 examines the accuracy of the previous research assumptions compared to the assumptions considered in this study. A parametric study is then conducted to examine the effect of boundary conditions on panel surfaces in terms of transient moisture load in Section 2.5.2. A combination of different wood species with PUR adhesive is modeled in Section 2.5.3 to check the effect of wood layers' diffusivity on the moisture profile of CLT.

The application of wood species for outer and middle layers of CLTs and different types of adhesive material are discussed in Sections 2.5.4 and 2.5.6, respectively, to investigate the moisture profile of CLTs with different wood species and different glue layers. The moisture exposure duration effect on MC is discussed in Section 2.5.7. Finally, the influence of orthotropic moisture diffusion coefficients and layers direction of CLTs on the moisture profile is presented in Section 2.5.8.

2.5.1 Influence of adhesive's diffusivity on moisture profile of CLT

In Section 2.2.3, the dependency of the material's diffusivity to moisture content (MC) and the moisture exposure time (t) was shown. Although previous research has shown that D varies with MC, conducting experimental studies to determine the exact variation of D with MC is quite challenging [2], [59]. One approach to address this challenge is defining mathematical relations to calculate moisture diffusion as a function of MC and t. However, this method is also based on experimental data. Therefore, previous research finding a unified way to simulate the moisture profile of composite materials without considering the variation of D is essential. For this purpose, two constant values for D_{adh} were estimated in some literature for adhesives [6], [27]. These constant values are approximately 500 to 50 times smaller than the diffusion coefficient of the wooden layers of CLT. In this section, a parametric study is completed to show the accuracy of the previous assumption according to Table 2.5 in calculating the moisture profile of CLTs.

Table 2.5: Values of parameters of glue layers for moisture diffusion analysis of spruce CLT panel as the input data of ANSYS.

	Case studies	Density [Table 2.3] (kg/m^3)	Diffusion coefficient (m^2/s)	Specific Heat Capacity [42] $(J/kg.K)$	Conductivity [Table 2.3] $(W/m.K)$
A)	$D_{adhesive} = \frac{1}{50} D_{Spruce}$ [27]	1	2.76×10^{-12}	33.6	9.27×10^{-11}
B)	$D_{adhesive} = \frac{1}{500} D_{Spruce}$ [27]	1	2.76×10^{-13}	33.6	3.59×10^{-11}
C)	D_{adh} [42]	1	4.01×10^{-12}	33.6	1.34×10^{-10}

Fig 2.15 shows the predicted moisture profile of the spruce CLT panel for three values of D_{adh} (see Table 2.5) once the panel is exposed to RH=65%-100% for 14 days. The obtained results proved that considering D_{adh} according to Case A and Case B based on previous research assumptions does not result in a moisture profile with a good match compared to Case C and measurement data.

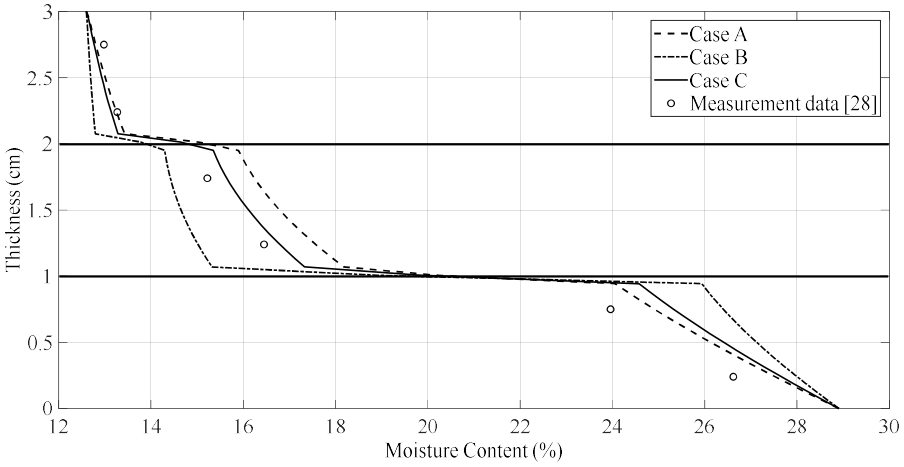

Fig 2.15: Moisture profile of spruce CLT exposed to 14 days moisture exposure considering various cases for moisture diffusion of glue lines according to Table 2.5.

2.5.2 Influence of boundary condition on moisture profile of CLT

In addition to glues' diffusivity effects, five additional cases were considered for both linear and nonlinear boundary conditions as the moisture flux in the Transient Analysis, based on the discussed method in Section 2.4.2. In the linear boundary condition, two values of c were calculated for RH=65% and RH=100%. Then, a linear boundary condition using the two c values was assigned to the interior surface of the model (see Fig 2.8). In the nonlinear boundary condition, the moisture adsorption curve is applied to the interior surface of the panel. Table 2.6 summarizes studied cases to investigate the effect of boundary conditions. Case 1 shows the moisture profile of the selected panel when D_{spruce} depends on moisture content, and D_{adh} remained constant under 14 days linear boundary condition. In Case 2, D of the selected CLT panel changes with the fluctuating moisture content under a 14-day linear boundary condition. Cases 3 and 4 are the same as Cases 1 and 2, respectively, but under nonlinear boundary conditions for a 14-day moisture exposure (see Fig 2.7). In Case 5, both D_{spruce} and D_{adh} remained constant, while the nonlinear boundary condition was used according to Fig 2.7.

Table 2.6: Case studies for boundary conditions' effect on the moisture profile of spruce CLT panel.

Case studies	Diffusion coefficient of spruce layers (m^2/s)	Diffusion coefficient of adhesive (m^2/s)	Boundary condition (kg/m^3)
Case 1	Depends on moisture content (Eq 2.3)	4.01×10^{-12} [42]	Linear
Case 2	Depends on moisture content (Eq 2.3)	Depends on moisture content (Eq. (4))	Linear
Case 3	Depends on moisture content (Eq 2.3)	4.01×10^{-12} [42]	Nonlinear (Fig 2.7)
Case 4	Depends on moisture content (Eq 2.3)	Depends on moisture content (Eq 2.4)	Nonlinear (Fig 2.7)
Case 5	2.76×10^{-12} [27]	4.01×10^{-12} [42]	Nonlinear (Fig 2.7)

Fig 2.16 demonstrates that Case 4 resulted in an acceptable moisture profile compared to experimental data. However, in the lack of experimental data for D variation with MC, a constant

value for *D* may be a reasonable estimate for comparison purposes. Therefore, Case 5 was selected as a benchmark case to develop a model for other composites. This parametric study aimed to investigate the errors in the moisture profile when the moisture adsorption curve was not applied as the boundary condition. The result showed that although using a linear boundary condition can qualitatively predict the moisture content in CLT panels, the moisture adsorption curve resulted in more accurate moisture content predictions. Hence, the constant moisture diffusion coefficient, along with the moisture adsorption curve as the imposed boundary condition, are selected for further parametric studies. It should be noted that this approach does not require moisture-dependent diffusion properties. Fig 2.17 compares the moisture profile of spruce CLT for Cases 1 and 2 (under linear boundary condition) and Cases 3 and 4 (under nonlinear boundary condition) with the benchmark case study (Case 5) to better understand the effect of boundary conditions on the moisture profile of CLT.

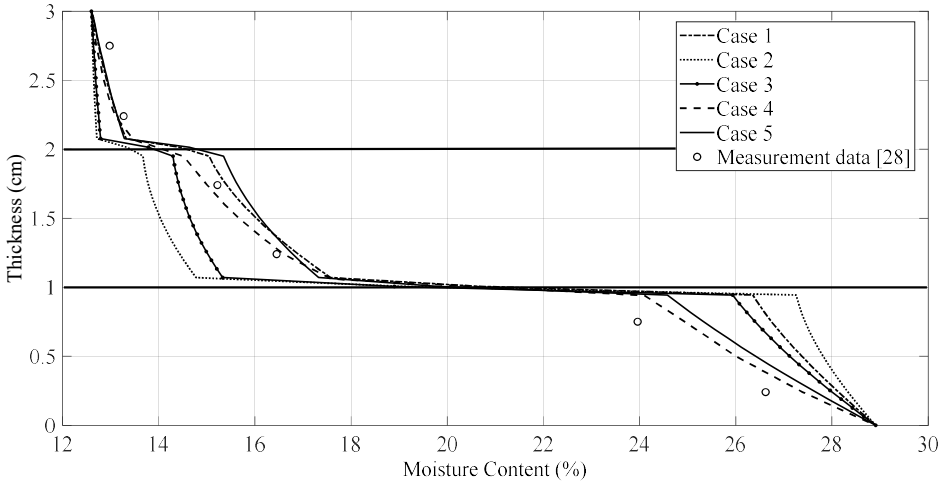

Fig 2.16: Results of case studies selected in numerical modeling of spruce CLT after 14 days of moisture exposure according to Table 2.6.

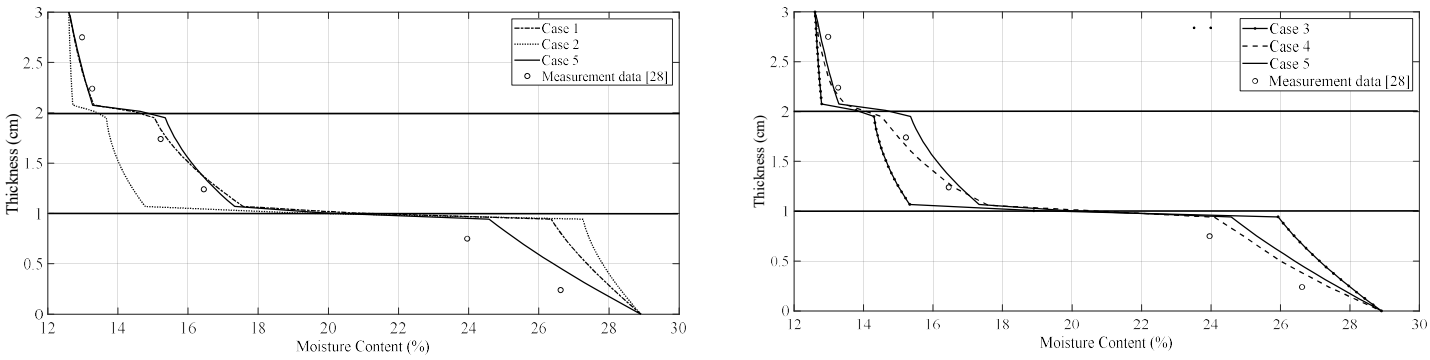

Fig 2.17: Moisture profile of spruce CLT panel for 14 days moisture exposure in the selected case studies according to Table 2.6. CLT is under: (a) linear boundary condition, (b) nonlinear boundary condition.

2.5.3 Influence of wood layers' diffusivity on moisture profile of CLT

Based on literature data, pine, balsa, and bamboo were selected to study the effects of wood species on laminated composite moisture profiles. The properties of these selected species are listed in Table 2.7, and their moisture adsorption curves are shown in Fig 2.18. The corresponding input values of these materials according to the thermal moisture analogy in ANSYS are listed in Table 2.8.

Table 2.7: Summary of Equilibrium Moisture Content (EMC), Moisture Concentration (c), and Moisture Diffusion Coefficient (D) values for spruce, pine, balsa, and bamboo.

Material	Density (kg/m^3)	EMC (%)	${c_{100}}^*$ (kg/m^3)	c_{65} (kg/m^3)	D (m^2/s)
spruce [27]	450	28.91	130.09	56.7	1.38×10^{-10}
pine [36], [38]	509	22.06	112.28	56.04	1.379×10^{-9}
balsa [34], [35], [39]	174	-	64.23	18.63	2.62×10^{-6}
bamboo [7–10]	1160	-	87.54	51.3	2.96×10^{-11}

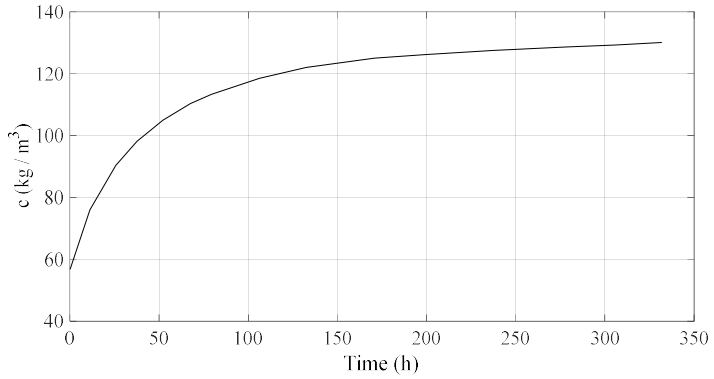

(a) spruce [27]

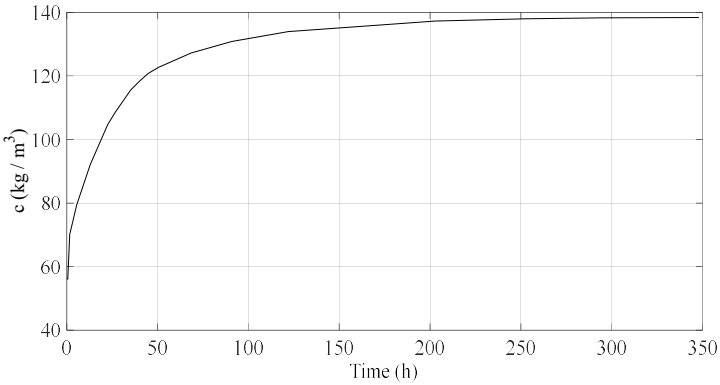

(b) pine [38]

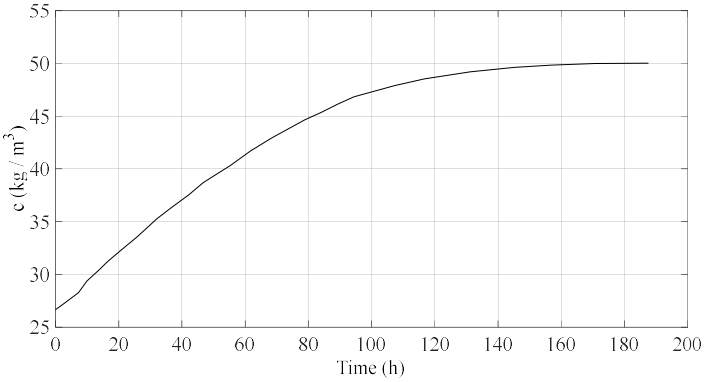

(c) balsa [35]

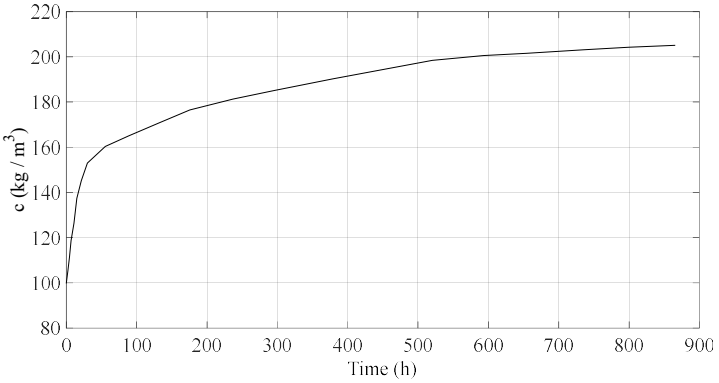

(d) bamboo [33]

Fig 2.18: Moisture adsorption of spruce, pine, balsa, and bamboo under the boundary condition (RH=65% to 100%) extracted from the literature.

The result of moisture diffusion across the cross-section of the studied panels is shown in Fig 2.19. The top layer of panels was exposed to RH=65%, and the bottom layer was exposed to RH= 100% for 14 days (336 h). Varying boundary conditions were imposed on the model according to the moisture adsorption curves of the selected materials (see Fig 2.18). The results show that moisture diffuses differently in various species based on their distinct cellular microstructures and hence their composites. When D_{adh} is smaller than the diffusion coefficient of the main layers, the moisture gradient between composite layers is significant (e.g. balsa composite). The moisture gradient becomes small when D_{adh} is close to D of the main layers' materials.

Table 2.8: Materials properties obtained from the thermal moisture analogy as the input data of ANSYS. (See Tables Table 2.2 and Table 2.7).

		Density (kg/m^3)	Conductivity $(W/m.K)$	Specific Heat Capacity $(J/kg.K)$	Diffusion coefficient (m^2/s)	Moisture concentration on the left side (Fig 6) (kg/m^3)	Moisture concentration on the right side (Fig 6) (kg/m^3)
Softwood	spruce	1	1.79×10^{-8}	130.09	2.76×10^{-12}	130.09	56.7
	pine	1	1.54×10^{-7}	112.28	2.74×10^{-11}	112.28	56.04
Hardwood	balsa	1	1.26×10^{-4}	48.37	5.24×10^{-8}	48.37	26.67
	bamboo	1	6.16×10^{-9}	208.22	5.92×10^{-13}	208.22	106.14
Adhesive (foamed)	PUR	1	1.34×10^{-10}	33.6	4.01×10^{-12}	-	-

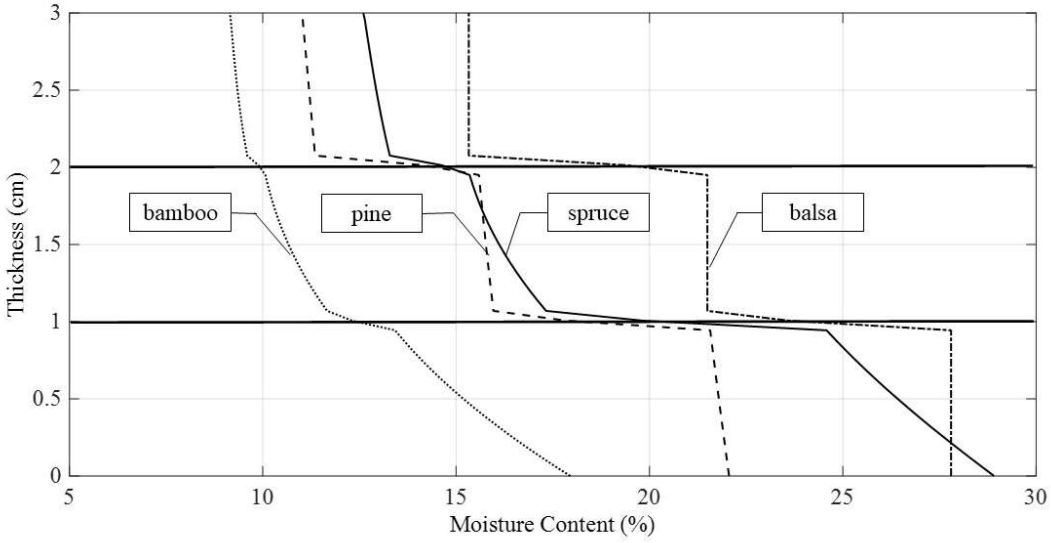

Fig 2.19: Moisture profile of laminated spruce, pine, balsa, and bamboo panels exposed to a humidity difference of 35% for 14 days. Material properties are listed in Table 2.7.

2.5.4 Influence of types of adhesives on moisture profile of CLT

In addition to the physical properties of the main layers' materials (i.e. *D*), adhesive properties also play a significant role in the moisture profile of CLTs. Fig 2.20 shows the moisture content variation in the cross-section of the thin adhesive layer in a three-layered spruce composite. Thus, it is expected changing the type of adhesive would change the moisture profile of CLT. First, the

model's sensitivity to the number of mesh elements in adhesive layers was examined. 1 and 3 number of elements were used per adhesive layer with a thickness of 0.1 mm. Once three elements were applied to adhesive layers, moisture content was affected by less than 0.006% (see Fig 2.20 (b)). As a result, the moisture profile of CLTs with thin adhesive layers is not influenced by the number of adhesive layers, and one element for adhesive layers was used for the rest of the modeling.

According to Section 2.5.3, bamboo CLTs result in a smoother moisture profile than other studied panels. This section uses a combination of bamboo with three different adhesive types (PUR, PRF, and PVAc) to investigate the adhesive type effect on the moisture profile of CLT.

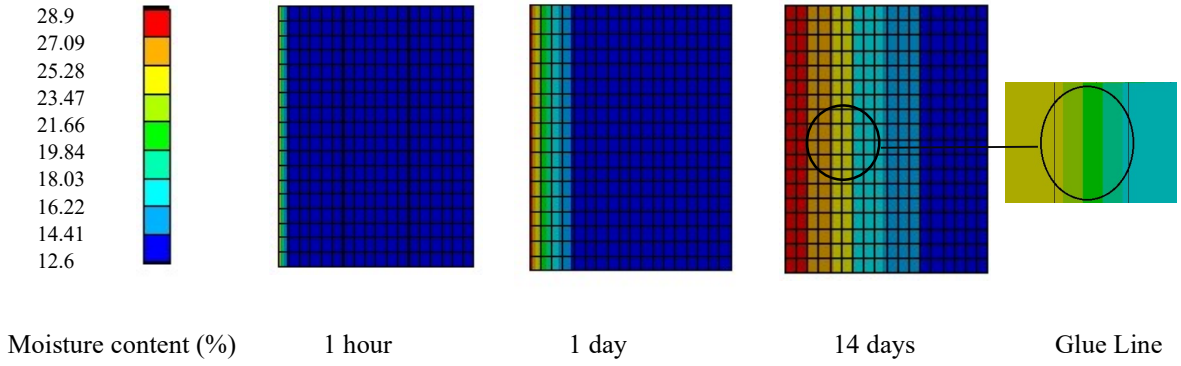

(a)

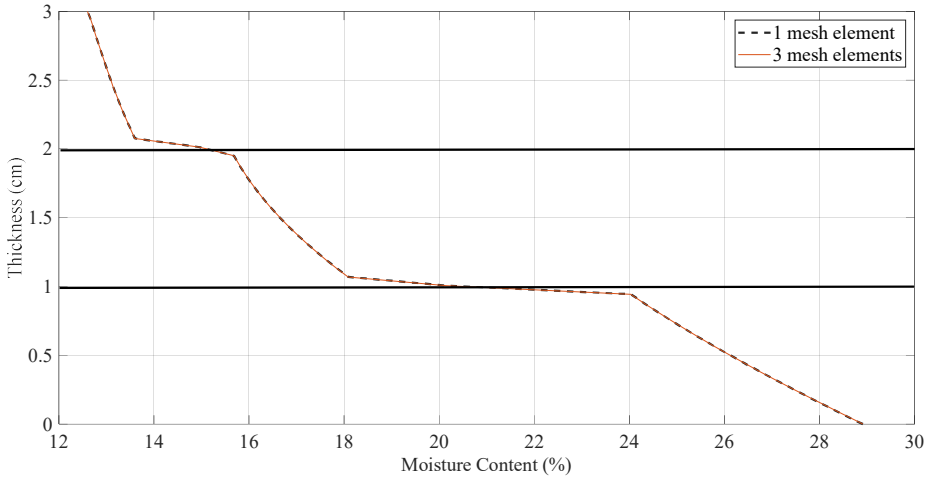

(b)

Fig 2.20: Moisture profile in three-layered spruce composite under 14 days moisture exposure, (a) moisture content variation in the cross-section of the adhesive layer, (b) model's sensitivity to the number of mesh elements in adhesive layers

Table 2.9 provides the moisture diffusivity of selected adhesive materials used in this section. Fig 2.21 indicates that using an adhesive with higher moisture diffusivity (PVAc) shows a lower moisture gradient at the glue lines. However, the resulting moisture content in the middle layer is a bit higher than other CLTs' moisture content.

Table 2.9: Moisture diffusivity of PVAc, PUR, and PRF adhesives *[42]*.

Material	D (m^2/s)
PVAc	17.8×10^{-12}
PUR	4.01×10^{-12}
PRF	0.58×10^{-12}

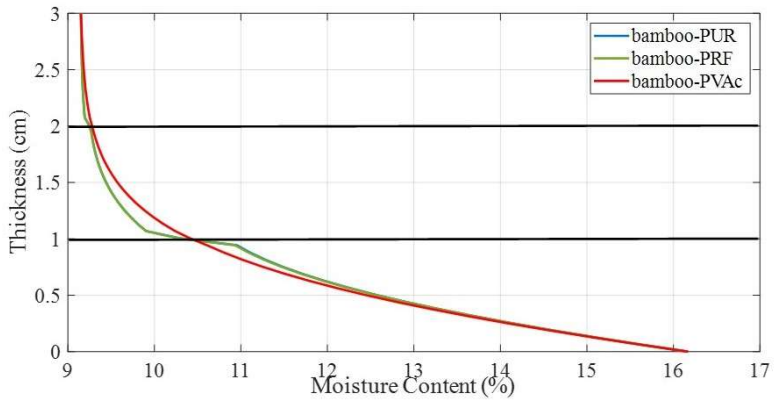

Fig 2.21: Type of adhesive effect on the moisture profile of bamboo CLT panels bonded with different adhesives (PUR, PRF, and PVAc) after 14 days of moisture exposure.

2.5.5 Influence of panel dimension on moisture profile of CLT

The described model in Section 2.4 was a small CLT three-layered spruce CLT ($40mm \times 80mm \times 30mm$). This section aims to show the panel dimension effect on the moisture profile. For this purpose, the validated model in Section 2.4.2 is developed for a large spruce CLT wall panel with a $2600mm \times 1500mm \times 30mm$ dimension. For comparison purposes, the panel's thickness remained constant as in the previous model. The result shows that the panel dimension does not influence the moisture profile. Because the moisture transfers in the cross-section of CLT panels (see Fig 2.22) and the required parameters in the thickness of the studied panels are the

same. So, the result of the moisture profile for both small and large panels is the same. However, changing the thickness of CLT panels will change the moisture profile of CLTs.

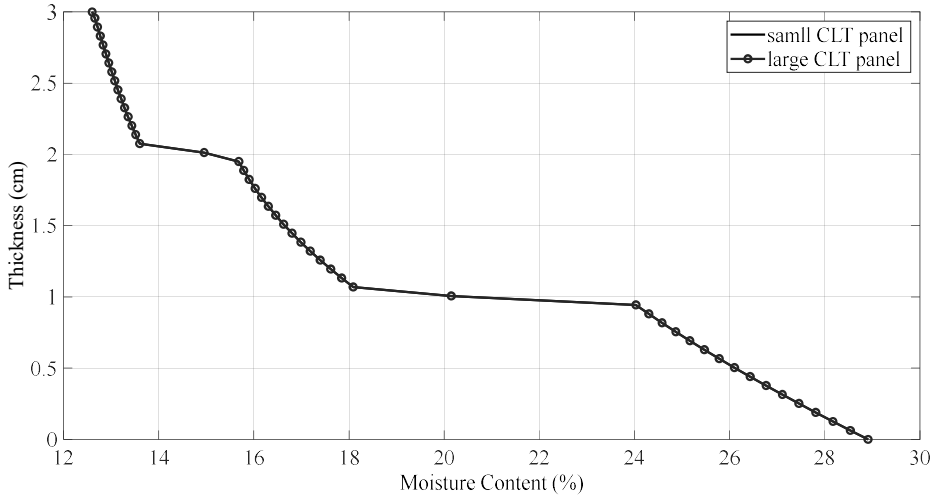

Fig 2.22: Moisture profile of small and large panels under 35% humidity difference for 14 days of moisture exposure.

2.5.6 Influence of different wood species on the moisture profile of CLT

The moisture transport in CLT panels with three different material layups was investigated to understand the layup effect. The material for the middle layer differed from the face layers; bamboo-pine-bamboo, spruce-balsa-spruce, and pine-balsa-pine were selected as three distinct layups with more porous middle layers. Layers are glued with PUR adhesive. Fig 2.23 shows the predicted moisture profile after 14 days of moisture exposure. Middle layers made from different materials had very distinct profiles, particularly in the middle. Results demonstrate that the higher diffusivity of the middle layer leads to the higher moisture content in the middle compared to the face layers. The very high moisture gradient found across the glue lines suggests that different species should be mixed with care in manufacturing laminated panels.

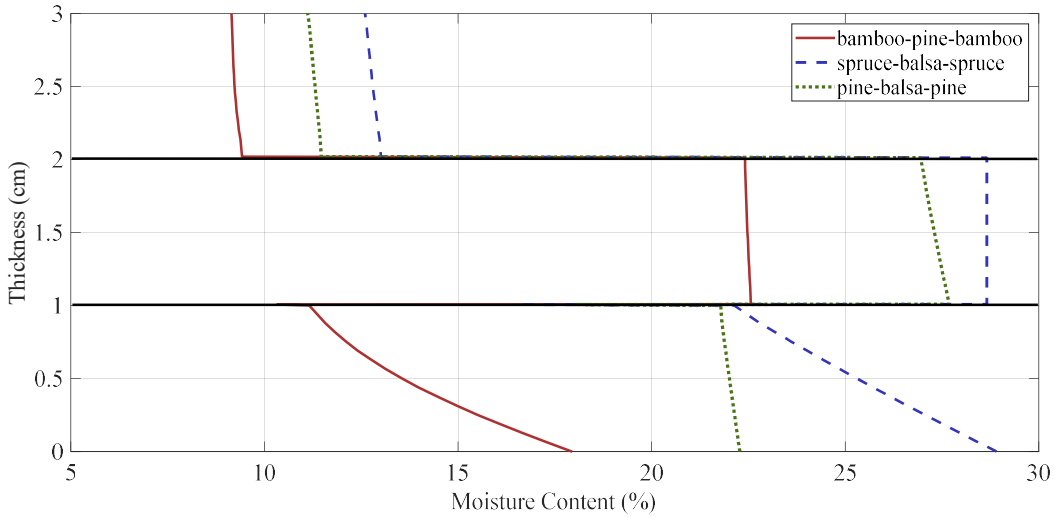

Fig 2.23: Layup effect on the moisture profile in three CLT panels with different species (bamboo-pine-bamboo, spruce-bamboo-pine, and spruce-balsa-pine) after 14 days of moisture exposure.

2.5.7 Influence of moisture exposure duration on moisture profile of CLT

This section discussed the long-term and short-term moisture profiles of CLT panels. For this purpose, spruce CLT panels glued with three different adhesives are modeled. The time duration of moisture exposure is considered 1 hour and 28 days. The result indicates the types of adhesives do not affect the short-term moisture profile of CLT panels. However, spruce-PVAc obtains a smoother moisture profile for long-term exposure than other modeled CLTs.

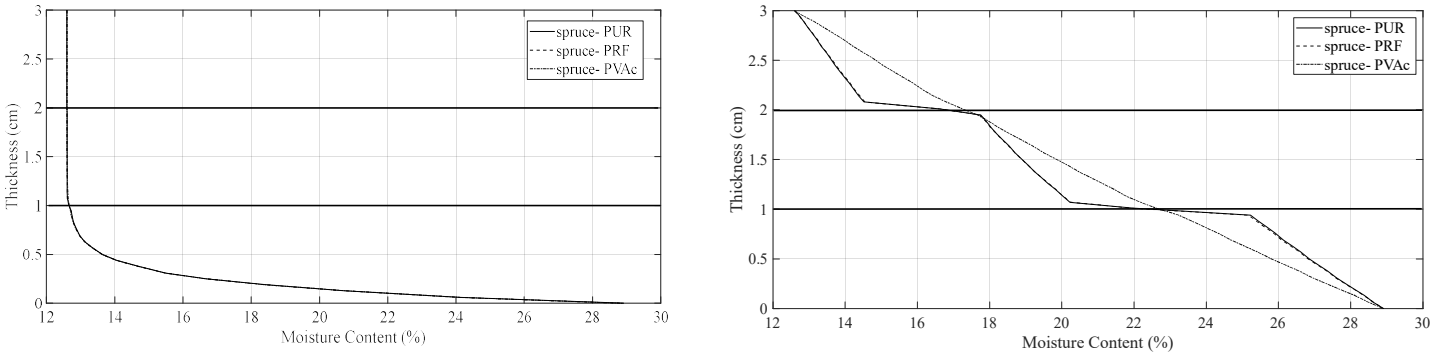

Fig 2.24: Effect of moisture exposure duration on moisture profile of three different spruce CLT panels, (a) 1-hour moisture exposure, (b) 28 days moisture exposure.

2.5.8 Influence of orthotropic diffusivity and layers direction on moisture profile of CLT

This section aims to investigate the effect of considering an orthotopic moisture diffusion coefficient for spruce on the moisture profile of CLT panels. Two different layers arrangement are considered for this purpose. CLTs with longitudinal directions for outer layers are considered parallel arrangements, and those with tangential directions are considered perpendicular arrangements. The detail of the layers' direction and the defined coordinate system are shown in Fig 2.25. PUR adhesive is used as the glue line material.

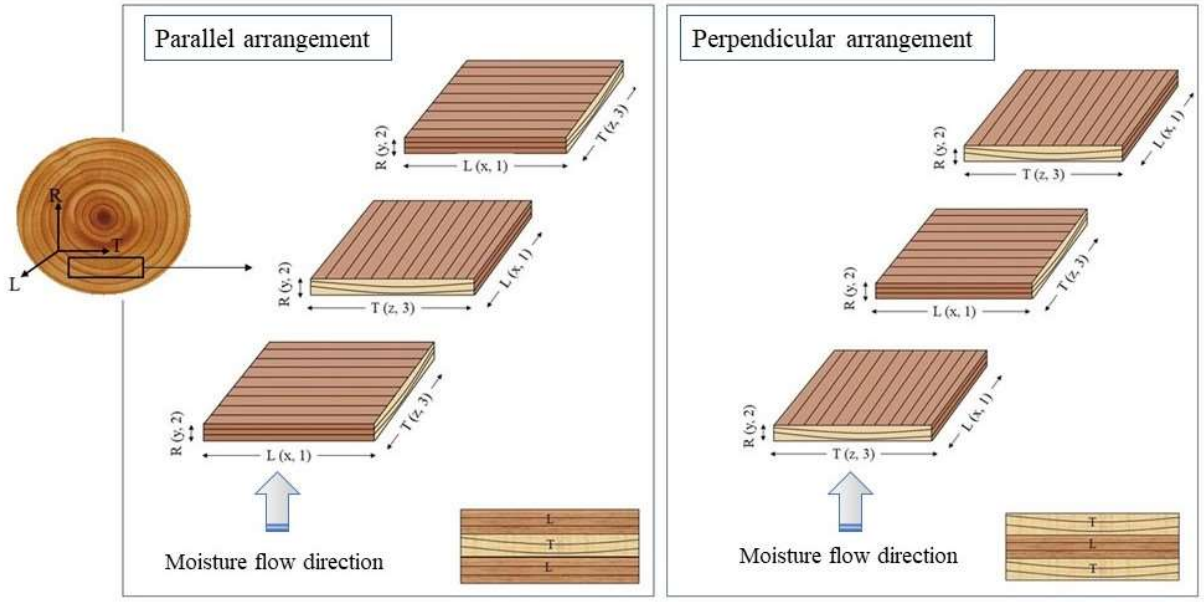

(a) (b)

Fig 2.25: Layers arrangement in CLT panels, (a) parallel arrangement, (b) perpendicular arrangement.

Rosenkilde [62] has reported the moisture diffusion coefficient of spruce materials in three directions based on the experiment according to Table 2.10.

Table 2.10: Moisture diffusion coefficient of spruce for T=20 °C and RH= 65% *[62]*.

Material	$\boldsymbol{D_L}\ (m^2/s)$	$\boldsymbol{D_R}(m^2/s)$	$\boldsymbol{D_T}(m^2/s)$
spruce	4.843×10^{-10}	1.968×10^{-10}	1.38×10^{-10}

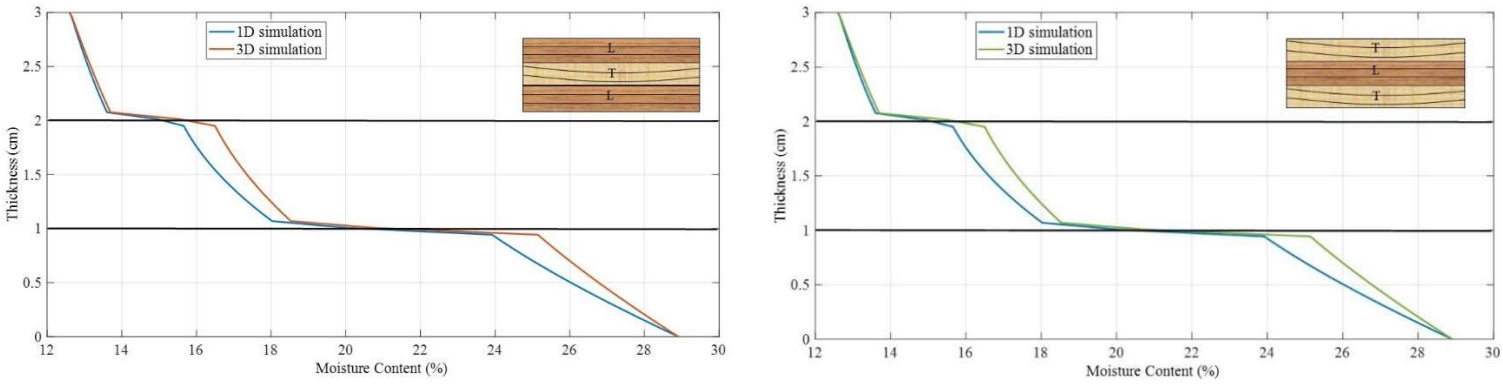

(a) (b)

Fig 2.26: Orthotropic diffusivity effect on moisture profile of spruce CLTs with different layers arrangement, (a) parallel arrangement, (b) perpendicular arrangement.

Fig 2.26 depicts 3D moisture profile results for spruce CLT panels with a different arrangement of layers. The results show that using orthotropic moisture diffusivity leads to a higher MC in CLT layers. However, the difference between results is not significant (4%), so considering moisture diffusivity in all directions equal to D_T is an acceptable assumption.

In addition, the moisture profile of CLTs with different layer arrangements shows no differences. Due to the constant condition of the model over the thickness of the panel, the result is as expected. Fig 2.27 shows the defined paths along the *x*, *y*, and *z* axes of the model. A model is subjected to two different boundary conditions in the *y* direction (see Fig 2.27, left) and in both the *y* and *z* directions (see Fig 2.27, right). The MC in the *x* and *z* directions does not change when the applied boundary condition is along the y axis, according to Fig 2.28.

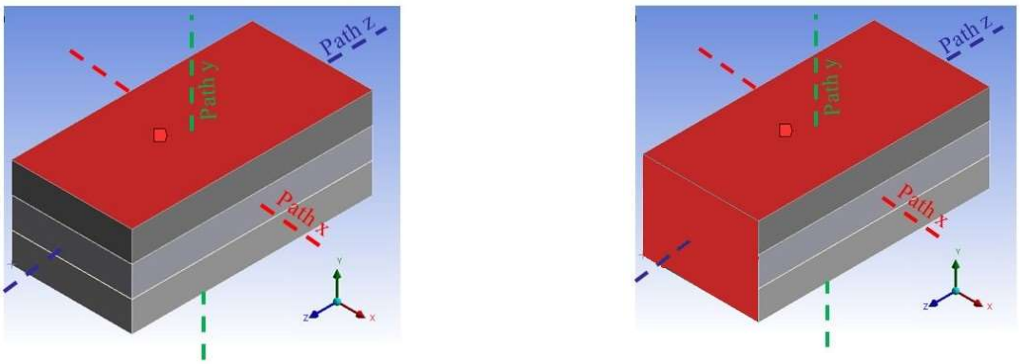

(a) (b)

Fig 2.27: Defined paths inside the CLT panels in x, y, and z directions, (a) applied boundary condition along y axis, (b) applied boundary condition along the y and z axes.

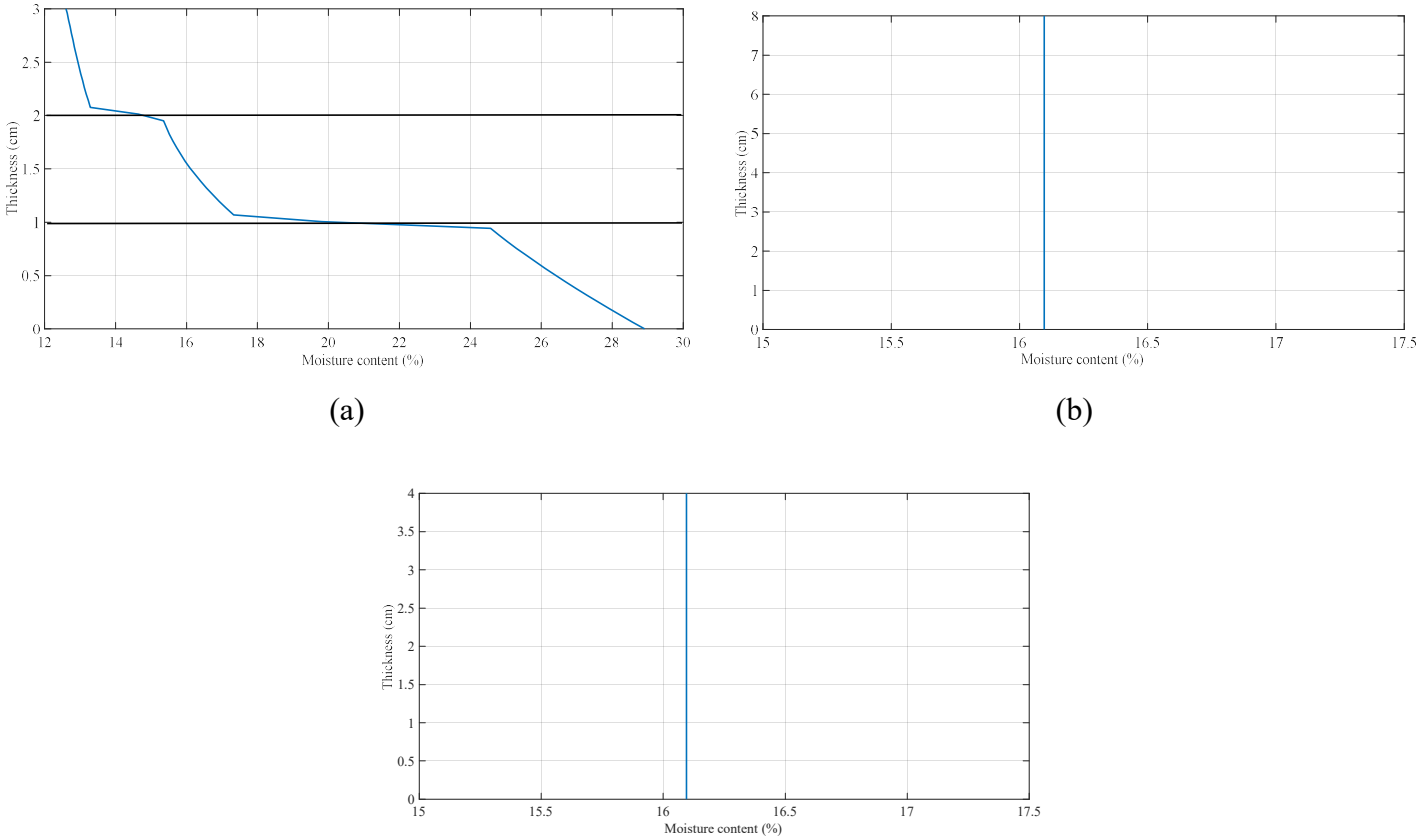

(a) (b)

(c)

Fig 2.28: Moisture profile of spruce CLT panel after 14 days moisture exposure in defined x, y, and z directions (according to Fig 2.27, a), (a) path y, (b) path z, (c) path x.

However, when an additional boundary condition is applied along the *z* direction, the MC in the *z* direction will be changed, according to Fig 2.29. According to this finding, the boundary condition at the edge of CLT panels should be considered in moisture transport models.

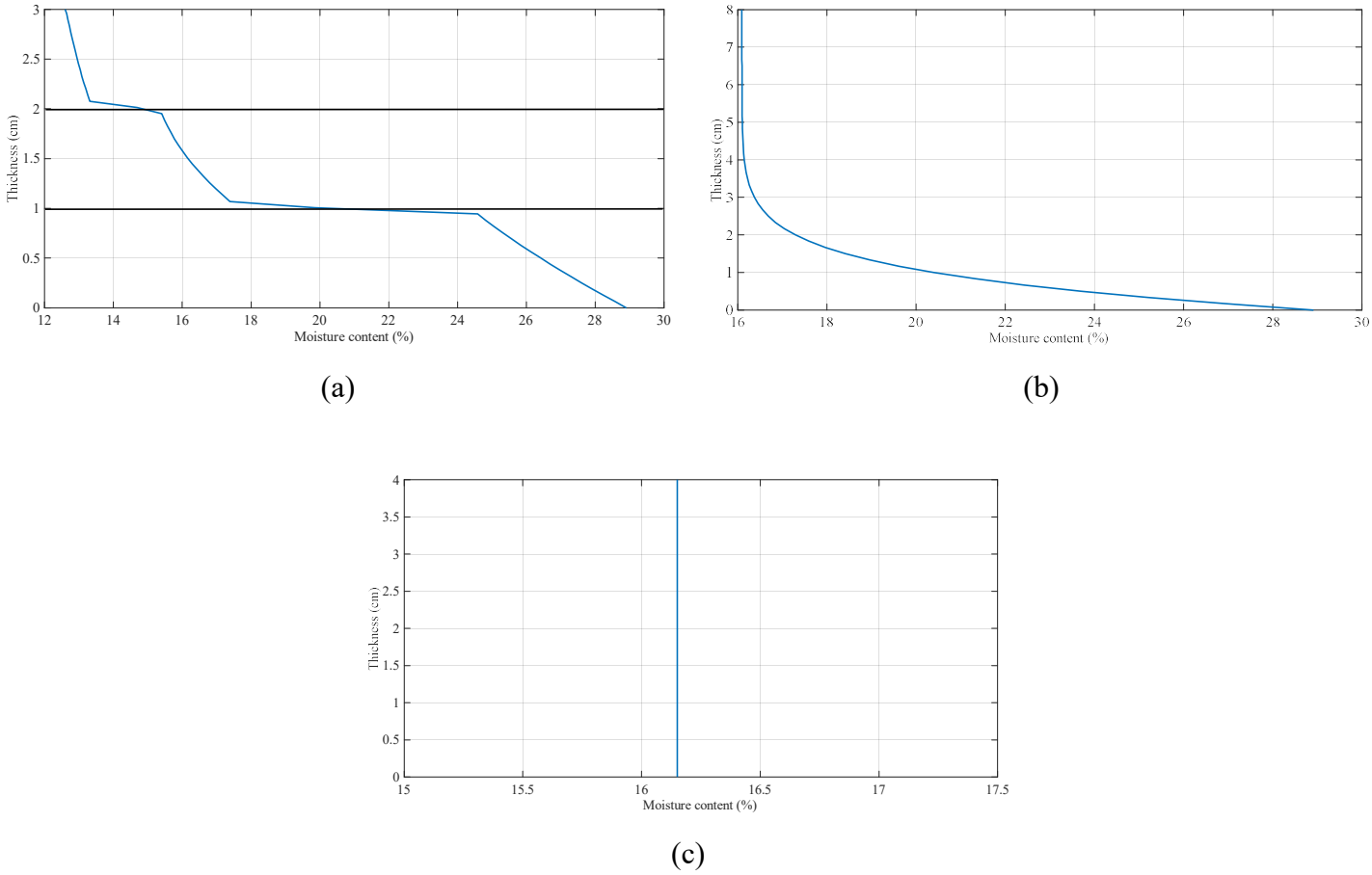

Fig 2.29: Moisture profile of spruce CLT panel after 14 days moisture exposure in defined x, y, and z directions, (according to Fig 2.27, b) (a) path y, (b) path z, (c) path x.

2.6 Conclusion

A comprehensive numerical study was conducted to simulate the moisture transport in various laminated composite panels. The panels were exposed to a relative humidity of 65% and 100% (on each side of the panel) for 14 days. The moisture adsorption curve of the material was prescribed as the boundary condition to conduct transient analysis. The result was verified by comparing it to previous experiments. It should be noted that since moisture adsorption and desorption curves of materials are not identical, further studies to investigate the effect of using the desorption curve as the prescribed boundary condition in the model are required for simulating cyclic scenarios. Although the previous studies showed that moisture diffusivity varies with the material's moisture content, this study demonstrated that such variation might not significantly affect the composite

panels' moisture profile. The generated moisture gradient at the glue lines might cause this due to the adhesive diffusivity.

Several parametric studies were completed to investigate how the moisture profile of CLT panels is affected by various parameters. The results showed that the assumption of previous research in considering D_{adh} approximately 500 to 50 times smaller than the diffusion coefficient of the wooden layers did not result in a good fit with experiments. The influence of adhesive types on moisture profiles proved that although variation of D_{adh} with moisture did not affect the results significantly, the magnitude of D_{adh} (compared to D of wood or bamboo) was identified to be a crucial parameter contributing to the moisture profile and the generated moisture gradient across the glue lines in CLT panels. When D_{adh} was smaller than the layers' D, the moisture gradient across the panel thickness was significant (e.g. in balsa composite). This matter led to large moisture gradients between layers. When D_{adh} was close to the main layers' D, the moisture gradient was found to be negligible, and a more uniform moisture profile was achieved. It could be concluded that depending on the selected wood or bamboo species, the proper choice of adhesive for manufacturing laminated panels can affect the moisture gradient across the glue lines later in the product's service life. However, it led to higher MC in the middle layer of CLT. When CLT panels are exposed to long-term moisture exposure, adhesive types can influence their moisture profiles. Also, the layup effect study indicated that the higher diffusivity of the middle layer leads to higher moisture content in this layer compared to face layers. The high moisture gradient noted across the glue lines suggests that different species should be mixed with care in manufacturing laminated panels. The 3D modeling of moisture transport in CLT panels revealed that using the tangential diffusivity for all directions is an acceptable assumption for moisture diffusion problems. This is consistent with similar assumptions made in [26]. Furthermore, the layer arrangements of CLT panels would affect the resulting MC under different boundary conditions.

3 Moisture-induced stresses in CLT

3.1 Introduction

Moisture-induced stresses generate once CLTs are exposed to fluctuating humidity. These stresses would lead to an expansion or a contraction depending on the CLT's moisture content compared to the ambient condition. Stresses perpendicular to the grain direction of wood are important as wood has a low tensile strength in this direction. This chapter presents the previous experimental study in measuring the moisture-induced stress perpendicular to the grain in the outer layer of CLT. The numerical model of the same specimen was developed, and the simulation result was compared with testing data to verify the model. After that, the model was developed for the other combination of CLTs (wood layers and adhesive) to perform parametric studies. Finally, a parametric study was completed to determine how adhesive properties (diffusivity and modulus of elasticity) influence stresses perpendicular to the grain direction of CLT.

3.2 Experiments

The results of an experimental study completed by Gereke [28] have been used in this study. Gereke measured the moisture-induced stresses in a three-layered spruce CLT glued by 1K PUR adhesive for a 50% relative humidity difference. Firstly, the specimen was conditioned at RH=35% for three days to reach a mass equilibrium. Afterward, it was transferred into a room with RH=85%. The measured moisture content of the outer and middle layers on different days has been reported in Table 3.1.

Table 3.1: Moisture content (%) in the outer and middle layers applied in the stress simulations *[28]*.

	Time (days)					
Layers	0	1	3	5	8	14
Outer layers	10.5	11.7	12.9	13.7	14.7	15.3
Middle layer	10.5	10.7	11.1	11.6	13.1	14.4

Fig 3.1 shows the procedure of the test. The specimen was divided into 200mm × 20mm strips after conditioning [28].

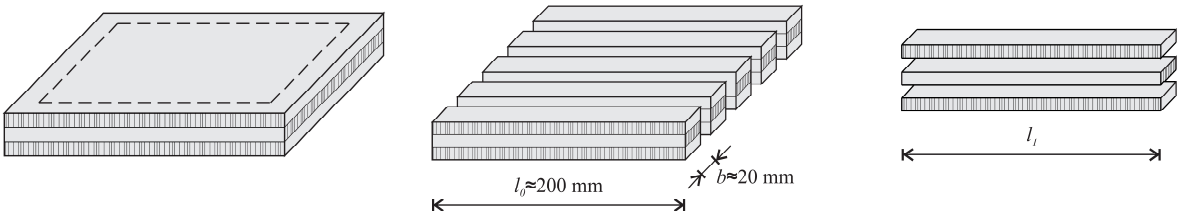

Fig 3.1: Procedure to determine the internal stress state of laminated wood panels, (a) removal of the edges, (b) cutting into strips, (c) release of strain by sawing in the glue lines [28].

The length of the strips was measured (l_0). Afterward, the layers were sliced into individual layers, and the length of the outer layer was measured as (l_1). The mean strain was calculated according to Eq 3.1, based on l_0 , l_1. The measured mean value for strain perpendicular to the grain (*zz* strain component) in the outer layer is reported in Fig 3.2, which is termed in ε_m in this thesis.

$$\varepsilon_m = \frac{l_0 - l_1}{l_0} \qquad \text{Eq 3.1}$$

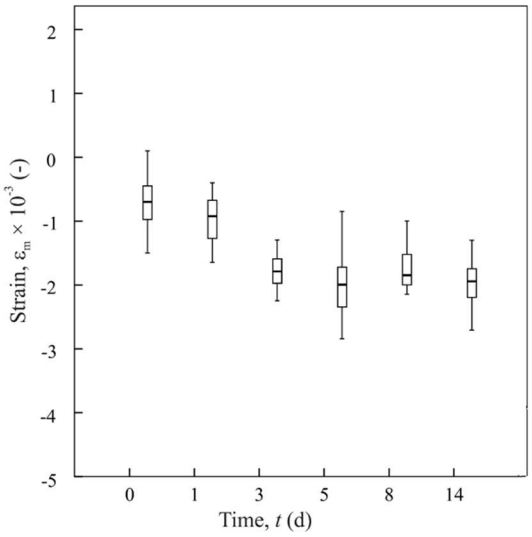

Fig 3.2: Mean strains perpendicular to the grain in the outer layers *[28]*.

An ultrasonic waves device was used to determine the modulus of elasticity in each layer. A transmitter and receiver were installed on each end of the slices, and the sound running time was measured over the layer length. Then, the layer elasticity was calculated through Eq 3.2.

$$E = \rho . C^2$$ Eq 3.2

where $C\ [m/s]$ is the measured sound velocity and $\rho[kg/m^3]$ is the spruce density. The measured modulus of elasticity for the outer layer is reported in Fig 3.3.

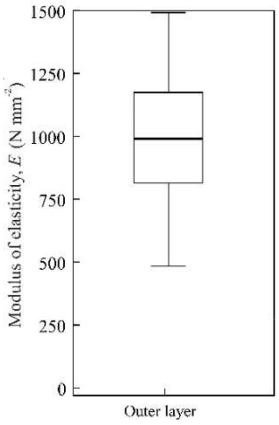

Fig 3.3: The measured modulus of elasticity in the outer layer of CLT *[28]*.

Finally, having the modulus of elasticity and mean strain, the mean stress perpendicular to grain was calculated according to Eq 3.3. The measured mean stress at each time duration is reported in Fig 3.4.

$$\sigma_m = E . \varepsilon_m$$ Eq 3.3

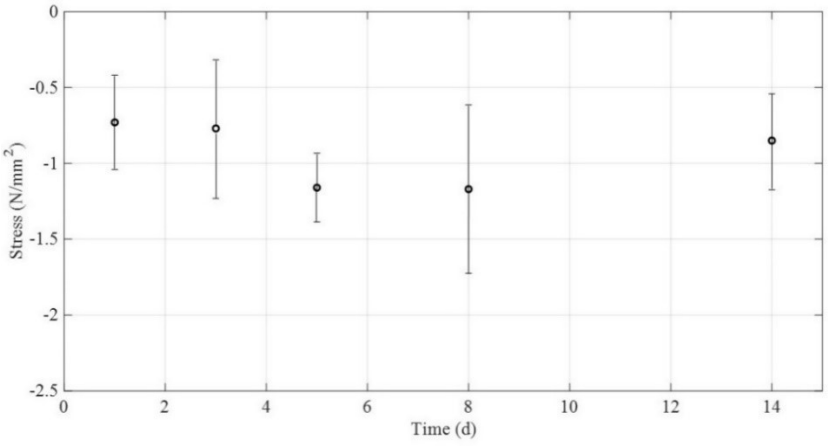

Fig 3.4: The measured mean stress perpendicular to the grain in the outer layer of spruce CLT *[28]*.

3.3 Numerical modeling

3.3.1 Material

According to the experimental study, spruce and 1K PUR adhesive were used in the modeling. The dependency of elastic coefficients of spruce to moisture content is displayed in Fig 3.5, Fig 3.6, and Fig 3.7.

.

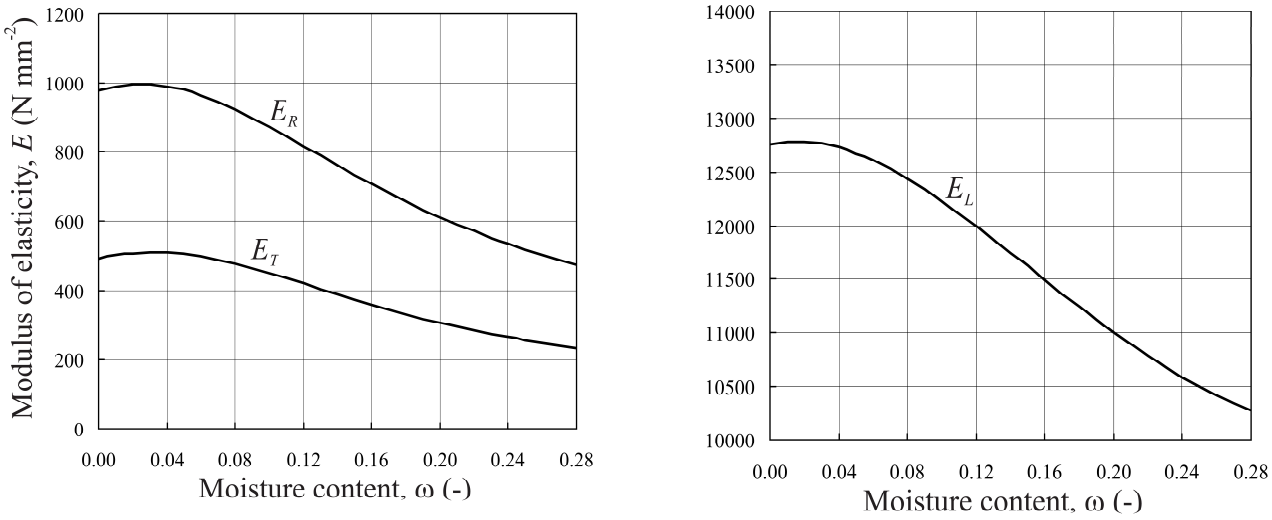

Fig 3.5: Modulus of elasticity E_L, E_R and E_T of spruce *[27]*.

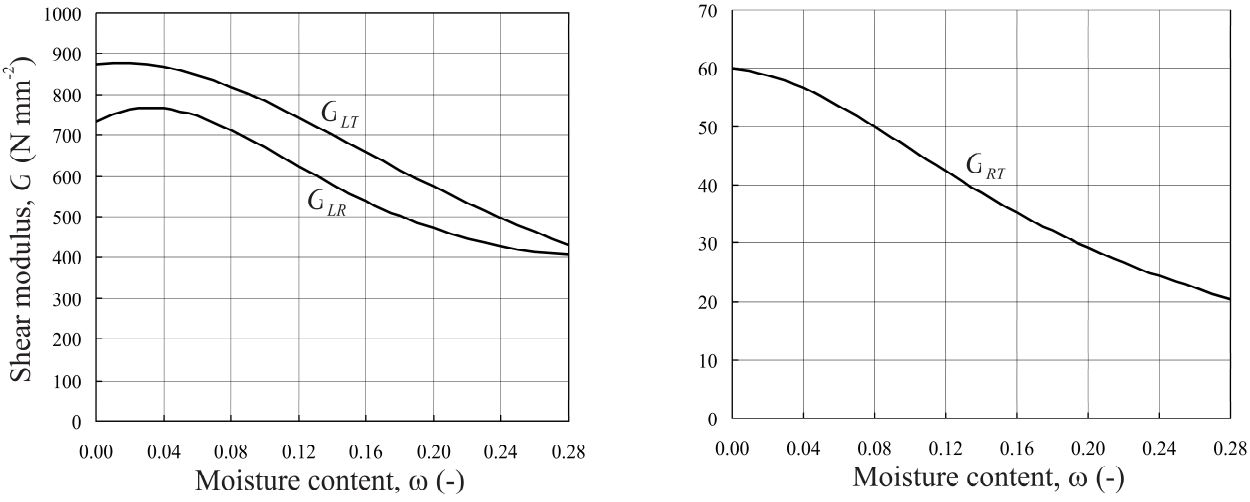

Fig 3.6: Shear Modul of G_{LR}, G_{LT}, and G_{RT} of spruce *[27]*.

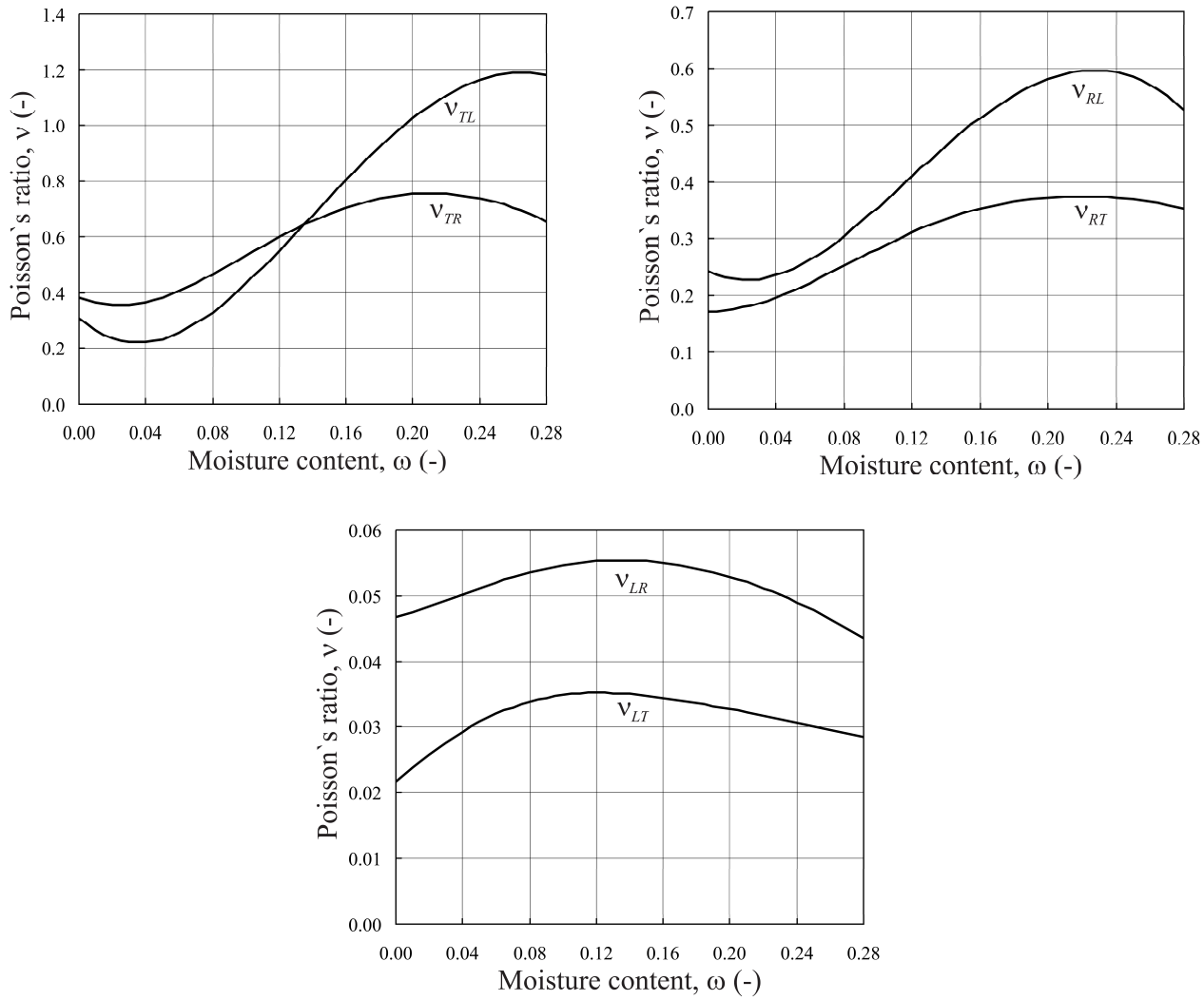

Fig 3.7: Poisson's ratios υ_{LR}, υ_{RT}, υ_{RL}, υ_{LT}, υ_{TL}, υ_{RT} and υ_{TR} of spruce *[27]*.

Table 3.2 summarizes the required materials' properties according to boundary conditions (RH=35% and RH=85%). Konnerth et al. [63] measured the elasticity modulus of 1K PUR using the tensile test and reported 0.36 GPa, 0.18 GPa, and 0.3 as Young's modulus, shear modulus, and Poisson's ratio, respectively.

Table 3.2: Summary of Equilibrium Moisture Content (EMC), Moisture Concentration (c), and Moisture Diffusion Coefficient (*D*) values for spruce and PUR adhesive.

Material	Density (kg/m^3)	EMC (%)	c_{85} (kg/m^3)	c_{35} (kg/m^3)	D (m^2/s)

spruce	450	28.91	77.4	35.6	1.38×10^{-10}
adhesive (PUR)	1000	3.36	33.6	22.2	4.01×10^{-12}

3.3.2 Method

Ormarsson [55] defined the total strain rate $\dot{\varepsilon}$ with respect to time as the sum of the elastic strain rate $\dot{\varepsilon}_{el}$, the moisture-induced strain rate $\dot{\varepsilon}_{w}$, and the mechano-sorptive strain rate $\dot{\varepsilon}_{w\sigma}$. This means that creep strain is not taken into account when the short-term behavior of materials is investigated [27].

The relationship between load and deformation is described by Hooke's law according to Eq 3.14:

$$\sigma = E.\varepsilon \qquad \text{Eq 3.4}$$

Replacing diverse modulus of elasticity (E^{-1}) with elastic compliance coefficient (S), Eq 3.14 is written as Eq 3.5 in the tensor format:

$$\varepsilon_{ij} = S_{ijkl}\,\sigma_{kl} \qquad i,j,k,l = 1,2,3 \qquad \text{Eq 3.5}$$

Due to the symmetry of the stress and the strain tensor, only 36 elastic coefficients are independent. Also, in an orthotropic material, like wood, tensor asymmetry implies that normal stress produces only normal strains, and shear stresses produce shear strains. Referring to the three principal axes L, R, and T to the indices 1, 2, and 3, Eq 3.5 may be written in Voigt notation as Eq 3.6:

$$\begin{bmatrix} \varepsilon_L \\ \varepsilon_R \\ \varepsilon_T \\ \gamma_{LR} \\ \gamma_{LT} \\ \gamma_{RT} \end{bmatrix} = \begin{bmatrix} s_{11} & s_{12} & s_{13} & 0 & 0 & 0 \\ s_{21} & s_{22} & s_{23} & 0 & 0 & 0 \\ s_{31} & s_{32} & s_{33} & 0 & 0 & 0 \\ 0 & 0 & 0 & s_{44} & 0 & 0 \\ 0 & 0 & 0 & 0 & s_{55} & 0 \\ 0 & 0 & 0 & 0 & 0 & s_{66} \end{bmatrix} \begin{bmatrix} \sigma_L \\ \sigma_R \\ \sigma_T \\ \tau_{LR} \\ \tau_{LT} \\ \tau_{RT} \end{bmatrix} \qquad \text{Eq 3.6}$$

The shear stresses (τ) link to shear strains (γ) by the shear modulus G. Also, Poisson's ratio υ_{ij} defines the ratio of the transverse strain ε_i (normal to the applied load) to the axial strain (in the direction of the applied load) in uniaxial tension or compression:

$$\upsilon_{ij} = \frac{\varepsilon_i}{\varepsilon_j}$$ Eq 3.7

Therefore, the elements of S tensor are defined as below using the elastic constants:

$S_{11} = E_L^{-1}$	$S_{22} = E_R^{-1}$	$S_{33} = E_T^{-1}$
$S_{44} = G_{LR}^{-1}$	$S_{55} = G_{LT}^{-1}$	$S_{66} = G_{RT}^{-1}$
$S_{12} = -\upsilon_{LR}S_{22}$	$S_{13} = -\upsilon_{LT}S_{33}$	$S_{23} = -\upsilon_{RT}S_{33}$
$S_{21} = -\upsilon_{RL}S_{11}$	$S_{31} = -\upsilon_{TL}S_{11}$	$S_{32} = -\upsilon_{TR}S_{22}$

Consequently, S matrix is defined as Eq 3.8:

$$S = \begin{bmatrix} E_L^{-1} & -\upsilon_{LR}E_R^{-1} & -\upsilon_{LT}E_T^{-1} & 0 & 0 & 0 \\ -\upsilon_{RL}E_L^{-1} & E_R^{-1} & -\upsilon_{RT}E_T^{-1} & 0 & 0 & 0 \\ -\upsilon_{TL}E_L^{-1} & -\upsilon_{TR}E_R^{-1} & E_T^{-1} & 0 & 0 & 0 \\ 0 & 0 & 0 & G_{LR}^{-1} & 0 & 0 \\ 0 & 0 & 0 & 0 & G_{LT}^{-1} & 0 \\ 0 & 0 & 0 & 0 & 0 & G_{RT}^{-1} \end{bmatrix}$$ Eq 3.8

Eq 3.14 is only valid if stresses and strains are related to the principal axes L, R, and T.

The elastic strain rate is obtained by differentiation of Eq 3.5 as:

$$\dot{\varepsilon}_{el} = S.\dot{\sigma} + \dot{S}.\sigma$$ Eq 3.9

The rate of change of S is determined according to Eq 3.10:

$$\dot{S} = \begin{bmatrix} -\frac{\dot{E}_L}{E_L^2} & \frac{\dot{E}_R \upsilon_{LR}}{E_R^2} - \frac{\dot{\upsilon}_{LR}}{E_R} & \frac{\dot{E}_T \upsilon_{LT}}{E_T^2} - \frac{\dot{\upsilon}_{LT}}{E_T} & 0 & 0 & 0 \\ \frac{\dot{E}_L \upsilon_{RL}}{E_L^2} - \frac{\dot{\upsilon}_{RL}}{E_L} & -\frac{\dot{E}_R}{E_R^2} & \frac{\dot{E}_T \upsilon_{RT}}{E_T^2} - \frac{\dot{\upsilon}_{RT}}{E_T} & 0 & 0 & 0 \\ \frac{\dot{E}_L \upsilon_{TL}}{E_L^2} - \frac{\dot{\upsilon}_{TL}}{E_T} & \frac{\dot{E}_R \upsilon_{TR}}{E_R^2} - \frac{\dot{\upsilon}_{TR}}{E_R} & -\frac{\dot{E}_T}{E_T^2} & 0 & 0 & 0 \\ 0 & 0 & 0 & -\frac{\dot{G}_{LR}}{G_{LR}^2} & 0 & 0 \\ 0 & 0 & 0 & 0 & -\frac{\dot{G}_{LR}}{G_{LR}^2} & 0 \\ 0 & 0 & 0 & 0 & 0 & \frac{\dot{G}_{LR}}{G_{LR}^2} \end{bmatrix} \quad \text{Eq 3.10}$$

The moisture-induced strain is released under the variation of moisture content. Shrinking and swelling occur as the moisture content of wood changes in response to changes in the relative humidity of the ambient air. The moisture-induced strain links to moisture content by a coefficient called swelling or shrinking material parameters (α) as Eq 3.11 [64]:

$$\varepsilon_w = \alpha \, . w \quad \text{Eq 3.11}$$

where α is defined in the orthotropic directions by α_L, α_R , and α_T as below:

$$\alpha = \begin{bmatrix} \alpha_L \\ \alpha_R \\ \alpha_T \\ 0 \\ 0 \\ 0 \end{bmatrix} \quad \text{Eq 3.12}$$

The values of α_L, α_R , and α_T are constant. Therefore, the rate of this strain is assumed to depend on the rate of change in moisture content according to Eq 3.13:

$$\dot{\varepsilon}_w = \alpha \, . \dot{w} \quad \text{Eq 3.13}$$

Suppose a wood specimen is under mechanical loading and moistening. In that case, it exhibits more significant deformation than the sum of the deformation of a loaded specimen under constant humidity conditions and the deformation of a non-loaded specimen [64]. This phenomenon is

called the mechano-sorptive effect. Ranta [65] investigated the mechano-sorptive strain rate as Eq 3.14:

$$\dot{\varepsilon}_{w\sigma} = m \,.\, \sigma \,.\, |\dot{w}| \qquad \text{Eq 3.14}$$

m is a mechano-sorption property that is obtained from experimental studies. The present study assumes that the total strain rate is the sum of the elastic and the moisture-induced strain rate. The mechano-sorptive strain is omitted from the material model since it is assumed that samples are not under mechanical loading.

In Fig 3.8, the element mesh, the geometry, and the coordinate system are given. The local coordinate system employed in the individual layers is rectangular. The longitudinal axis of these local coordinate systems is aligned parallel to the *x*-axis in the outer layers and parallel to the *z*-axis in the middle layer. The dimension of the tested CLT was $200mm \times 200mm \times 30mm$. Due to the panel's double symmetry, one quarter of the panel is modeled. Thus, two planes of symmetry and appropriate boundary conditions are applied. Considering 0.1 *mm* thickness for each glue line, the total dimension of the model will be $100mm \times 100mm \times 30.2mm$.

The moisture content applied to the model's middle and outer layers is obtained from the experiment. Table 3.1 gives the value of mean moisture content for 0, 1, 3, 5, 8, and 14 days of moisture exposure duration. Two paths along the *z*-axis are defined at $y = 0$ *mm* and $y = 10mm$ at the center of the panel (i.e. x=100 *mm*). The first path is placed at the bottom of the panel, and the second is situated directly at the glue line in the bottom layer.

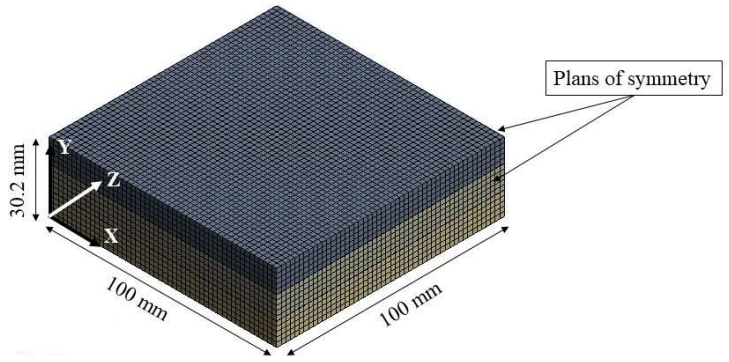

$$u_x = 0 \qquad at\ (100, y, z)$$
$$u_z = 0 \qquad at\ (x, y, 100)$$
$$u_x = u_y = u_z = 0 \qquad at\ (100,0,100)$$

Fig 3.8: Geometry of the model and boundary conditions.

3.3.3 Results

The predicted stresses over the defined paths in Section 3.3.2 are used to calculate the mean stress perpendicular to the grain of the outer layer. The average stress in the z-direction along both paths is reported as the mean stress perpendicular to the grain in the bottom layer. The results of predicted and measured stresses are shown in Fig 3.9. Gereke [28] modeled the same experiment, and his modeling results have been added to the result for comparison. Fig 3.4 shows a good agreement between simulations and measured stresses.

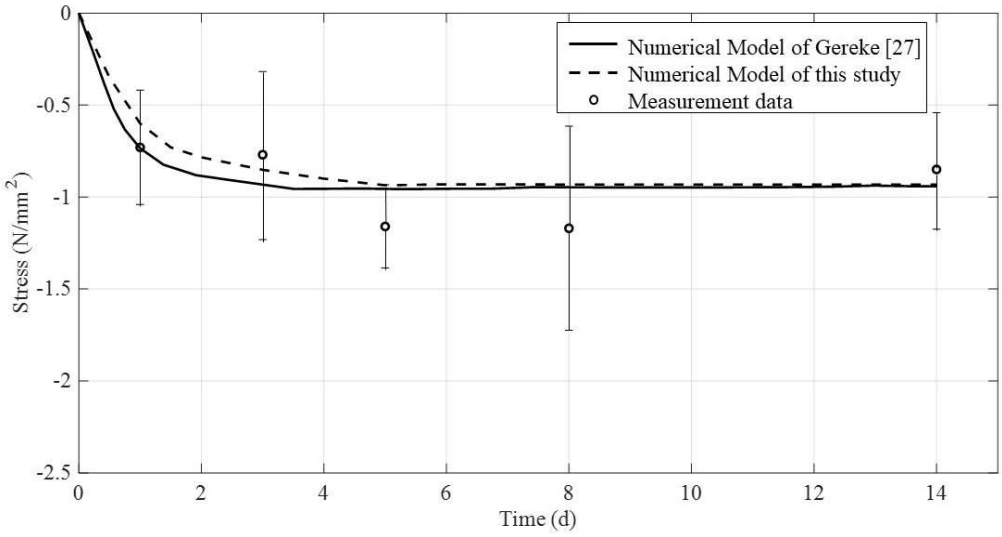

Fig 3.9: Simulated mean stress perpendicular to the grain in the outer layer of spruce CLT.

3.4 Parametric studies

The validated model in Section 3.3.3 can be used to investigate the influence of adhesives' properties on the stress perpendicular to the grain direction of different CLT panels. In Section 3.4.1, combinations of wood species and adhesive layers are selected to see the effect of different moisture profiles of CLTs on the stress state. Then, the widely used CLT panels in North American countries were added to selected materials to compare the result of stresses. In Section 3.4.2, moisture-induced failure analyses were conducted on various CLTs. Finally, the effect of the adhesive's diffusivity and elasticity on the stress perpendicular to the grain direction of CLTs was discussed in Sections 3.4.3 and 3.4.4.

3.4.1 Influence of moisture profile on the stress of CLT

In Section 2.5.4 , it was shown that adhesives with a higher diffusivity result in a lower moisture gradient at glue lines. Table 3.3 lists different adhesive materials that are frequently used as wood adhesives. The higher and lower diffusion coefficient is observed in PVAc (polyvinyl acetate) and PRF (phenol–resorcinol–formaldehyde), respectively.

Table 3.3: Moisture diffusion coefficient of various adhesive materials *[42]*.

Adhesive material	D (m^2/s)
PVAc	17.8×10^{-12}
PUR S709	4.9×10^{-12}
PUR S309	4.01×10^{-12}
MUF	1.37×10^{-12}
Fish Glue	0.9×10^{-12}
PRF	0.58×10^{-12}

Fig 3.10 indicates the relation between wood species' properties (strength and diffusivity) and their density. The diffusion coefficient of wood is lower in denser species. On the other hand, the strength of wood species increases linearly with their density, as shown in Fig 3.10. Oak and pine with tensile strength perpendicular to the grain direction of 5.5 MPa and 7.5 MPa, respectively, are selected for this case study.

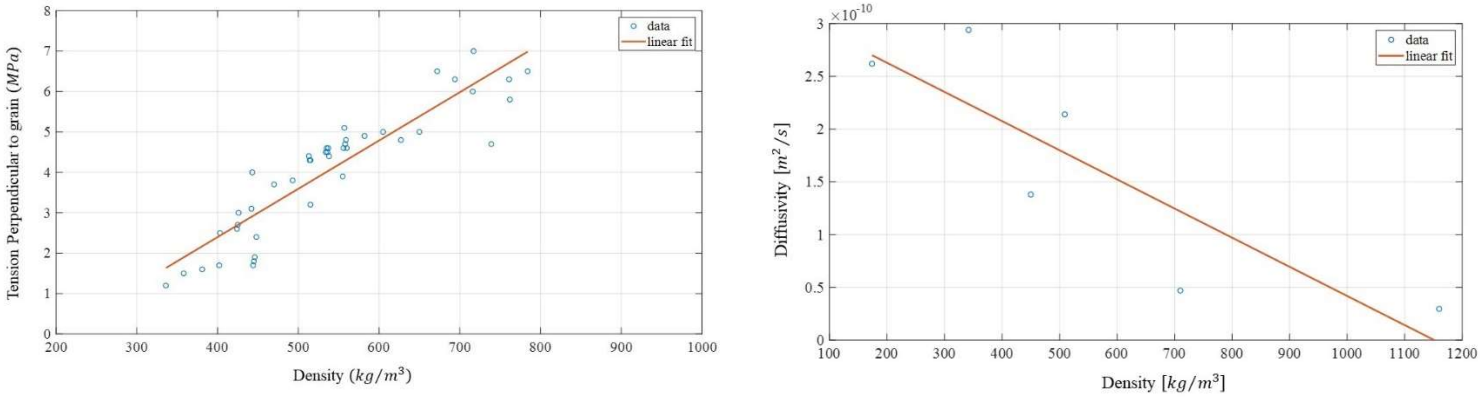

(a) (b)

Fig 3.10: Wood species properties, (a) tensile strength perpendicular to gain versus density, (b) moisture diffusion coefficient versus density.

Four combinations of oak and pine wood layers with PVAc and PRF adhesives are selected: pine-PVAc, pine-PRF, oak-PVAc, and oak-PRF. Fig 3.11 shows the result of moisture transport in the cross-section of these CLTs based on Section 2.4.2. The result indicates that a higher moisture gradient appears at the place of the glue line in the pine-PRF panel compared to other CLTs. The oak-PVAc combination resulted in a smoother moisture profile with less moisture gradient at the glue line.

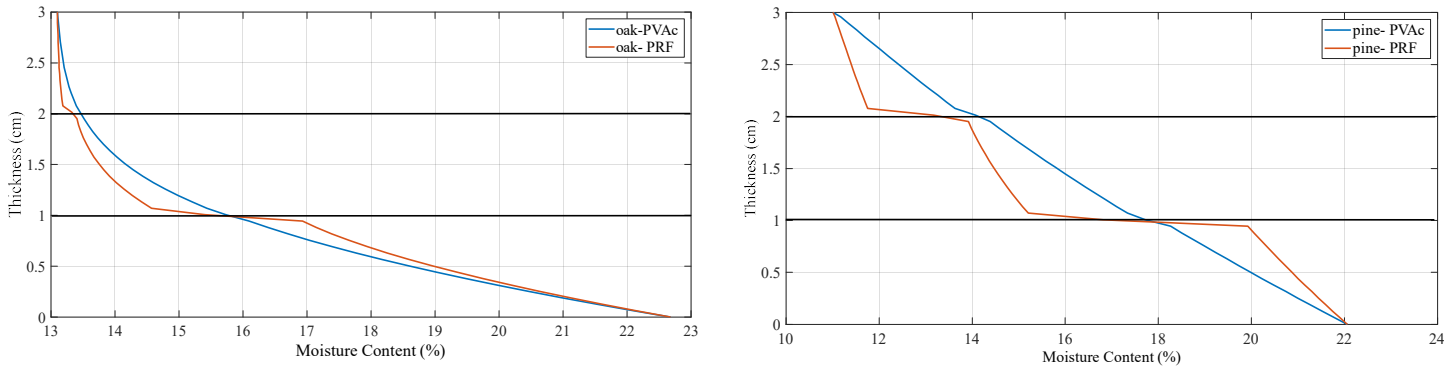

Fig 3.11: Moisture profile of four different CLT species, oak-PVAc, oak-PRF, pine-PVAc, and pine-PRF.

To investigate the influence of moisture profile on stress perpendicular to the grain direction of CLT, a $200mm \times 200mm \times 30.2mm$ panel with three support points at ($50mm$, 0, $100mm$), ($150mm$, 0, $50mm$), and ($150mm$, 0, $150mm$) is simulated over 14 days of moisture exposure. The initial condition for the simulations is set to RH=65%. The moisture profile simulation is conducted according to Section 2.4.2, and the stress simulation is completed based on Section 3.3.2. The fiber direction of the outer layers is along the x-direction, and the fiber direction of the middle layer is along the z-direction.

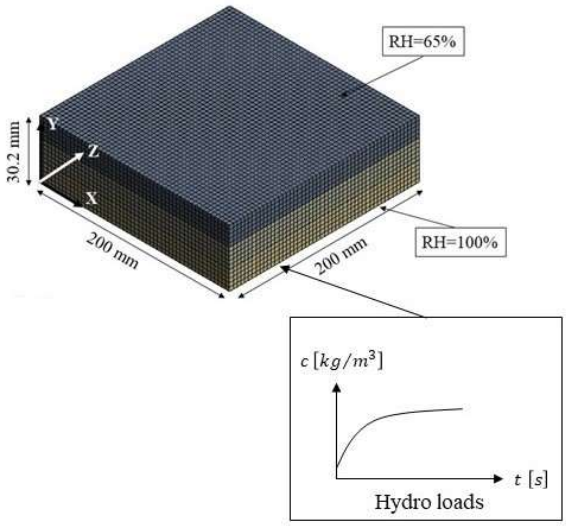

$$at \begin{cases} (50,0,100) \\ (150,0,50) \\ (150,0,150) \end{cases} \rightarrow u_x = u_y = u_z = 0$$

Fig 3.12: Geometry of the model and boundary conditions.

The elastic constant of the wood species and glues selected for this study are given in Table 3.4 and Table 3.5, respectively.

Table 3.4: The elastic constants of the selected materials; oak, pine, and spruce.

Material	Moisture content (%)	Young's modulus (GPa)			Shear modulus (GPa)			Poisson's ratio (-)		
		E_T	E_L	E_R	G_{LR}	G_{RT}	G_{LT}	ν_{LR}	ν_{TR}	ν_{TL}
oak [46], [66]	12	0.56	7.85	1.28	1.29	0.39	0.76	0.37	0.62	0.43
pine [46], [67]	12	0.616	13.5	1.2	0.78	0.079	0.836	0.379	0.334	0.366
spruce [27], [46]	12	0.397	12.8	0.625	0.617	0.053	0.587	0.018	0.48	0.45

Table 3.5: The elastic constants of the selected adhesives; PVAc, PRF, and PUR *[63]*.

Material	Young's modulus (GPa)	Shear modulus (GPa)	Poisson's ratio (-)
PVAc	1.1	0.6	0.34
PRF	3.5	1.2	0.36
PUR	0.36	0.18	0.3

Fig 3.13 shows the mean stress perpendicular to grain direction (σ_{zz}) over the thickness of the selected CLTs. The result indicates that the higher moisture gradient at the place of the glue line leads to higher stress at the glue lines and vice versa; the lower moisture gradient results in lower stress at the glue lines. The bottom layer of the pine-PRF panel with higher MC than the middle layer tends to expand. So, the compression stress occurs at the bottom glue line. On the other hand,

the upper layer of pine-PRF tends to contract due to lower MC than the middle layer, resulting in tensile stresses at the upper glue line.

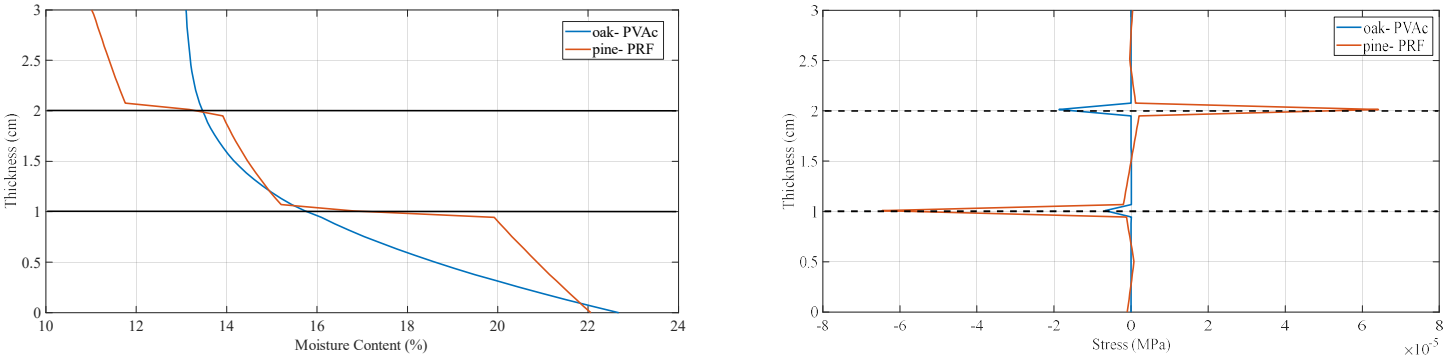

(a) (b)

Fig 3.13: (a) moisture profile of oak-PVAc and pine- PRF, (b) Simulated stresses perpendicular to the grain over the thickness and on the center path of CLT oak-PVAc and pine-PRF.

Two different paths are defined at the center of the panel for the outer layer in y=0 *mm* and y=10 *mm*, to study the stress state (σ_{zz}) along the outer layer of panel length. The same approach is followed for the middle layer by defining paths at y=10.1 *mm* and y=20.1 *mm*. The mean value of stress in the z-direction for outer layer paths is reported as the stress perpendicular to the grain direction of the outer layer. For the middle layer, the stress values in the x-direction are reported. Fig 3.14 displays the simulated stress perpendicular to grain direction in the middle and outer layers of oak-PVAc and pine-PRF panels. As indicated in Fig 3.13, the amount of MC in the middle and outer layers of the pine-PRF panel is higher than the moisture content in oak-PVAc. Due to the higher MC, the pine-PRF panel showed higher stress in its middle and outer layers than the oak-PVAc panel.

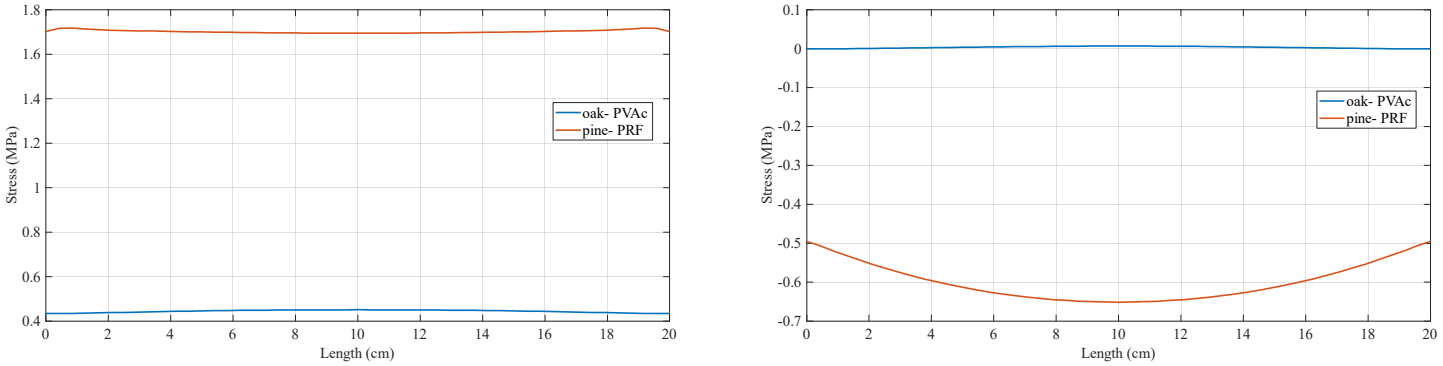

(a) (b)

Fig 3.14: Stress perpendicular to grain (σ_{zz}) over the length of oak-PVAC and pine-PRF, (a) middle layer, (b) outer layer.

Two extra panels widely used in the construction industry, spruce-PUR and pine-PUR, are added to the model for comparison purposes. The moisture profile and stress over the thickness of the studied panels are displayed in Fig 3.15. The results show the significant differences between the spruce-PUR panel and other CLTs. Because the spruce-PUR panel has a higher MC than other panels, it experiences a higher stress level.

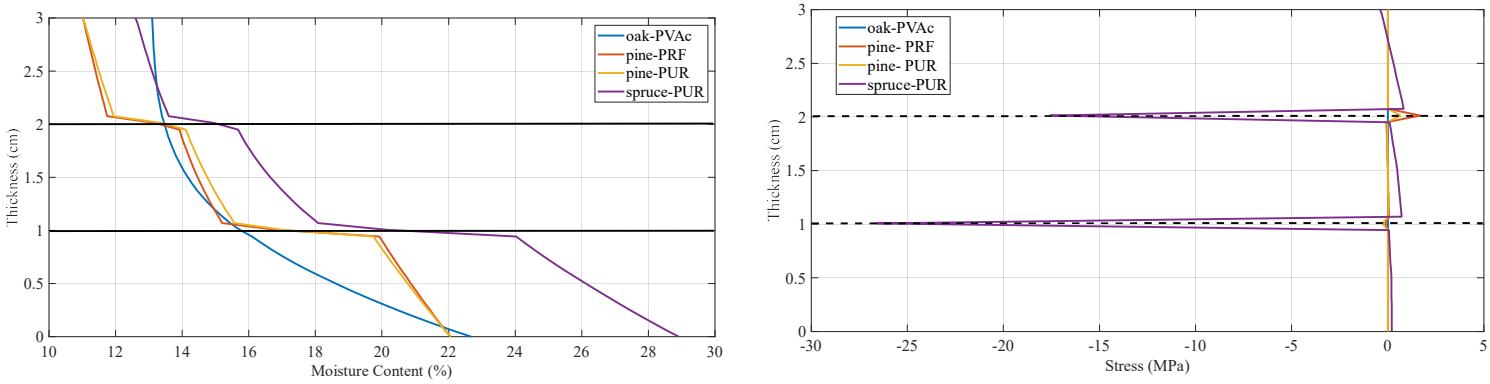

(a) (b)

Fig 3.15: (a) moisture profile of selected CLTs, (b) Simulated stresses perpendicular to the grain over the thickness and on the center path of selected CLTs.

3.4.2 Influence of wood strength on CLT failure

The orthotropic properties of wood layers in CLT panels lead to a complex behavior of CLT [68]. Ductile and brittle failure modes can simultaneously occur in wood layers [69]. Understanding this complex behavior of wood in parallel and perpendicular to the grain directions is paramount to

having a safe and reliable application of CLT in structural systems. Researchers have proposed various failure criteria to identify the failure modes. The selected failure criteria for this study are based on Tsai-Wu [70] model, which is widely used in the timber research community. For a complete 3D description of wood as an orthotropic material, eight stress-based failure criteria have been defined, with f_x being material strengths in tension (index t), compression (index c), and shear (index υ and roll) in parallel (index 0) and perpendicular (index 90) directions, as below [70]:

- $\sigma_L \geq 0$ - Criterion I: Failure in tension parallel to grain is a brittle failure mode of wood that is caused by tensile stresses σ_L parallel to grain. It is assumed that other stress components do not influence the tensile strength parallel to grain. The maximum stress criterion is:

$$F_{t,0}(\sigma) = \frac{\sigma_L}{f_{t,0}} \leq 1 \qquad \text{Eq 3.15}$$

- $\sigma_L < 0$ - Criterion II: Failure in compression parallel to grain is a ductile failure mode of wood that is caused by compression stresses σ_L parallel to grain. The maximum stress criterion is:

$$F_{c,0}(\sigma) = \left|\frac{\sigma_L}{f_{c,0}}\right| \leq 1 \qquad \text{Eq 3.16}$$

The transverse tension modes and shear modes must be combined as splitting parallel to the LR-plane can be caused by tension perpendicular to grain (mode I), shear (mode II), or a combination of both (mixed mode). It is not possible to define separate failure modes for each stress component as degradation of one component also leads to degradation of the other components. This means that damage due to longitudinal shear also leads to damage in tension perpendicular to grain even though the actual normal tension stress component perpendicular to grain may still be lower than the transverse tensile strength.

- $\sigma_{R/T} \geq 0$ - Criteria III / IV: Failure in tension perpendicular to grain with splitting in LT and LR plans, respectively. It is a brittle failure mode of wood that is caused by tensile stresses $\sigma_{R/T}$ in the perpendicular direction, longitudinal shear stresses $\sigma_{LR/LT}$ in the LT plane or rolling shear stresses σ_{RT}:

$$F_{t,90R/T}(\sigma) = \frac{\sigma_{R/T}^2}{f_{t,90}^2} + \frac{\sigma_{LT/LR}^2}{f_{\upsilon}^2} + \frac{\sigma_{RT}^2}{f_{roll}^2} \leq 1 \qquad \text{Eq 3.17}$$

- $\sigma_{R/T} < 0$ - Criteria V / VIII: Two failure modes, "pure transverse compression" and "shear", both occurring under compression perpendicular to grain, are distinguished. Failure in compression perpendicular to grain is a ductile failure mode of wood which is caused only by compression stresses $\sigma_{R/T}$ in the perpendicular direction. Brittle shear failure can also occur if, for instance, the compression load is applied with an angle to the grain, creating high shear stress components. Therefore, also a failure criterion for high shear stresses under simultaneous compression perpendicular to grain must be introduced:

$$F_{c,90R/T}(\sigma) = \left|\frac{-\sigma_{R/T}}{f_{c,90}}\right| \leq 1 \qquad \text{Eq 3.18}$$

$$F_{\upsilon R/T}(\sigma) = \frac{\sigma_{LT/LR}^2}{f_\upsilon^2} + \frac{\sigma_{RT}^2}{f_{roll}^2} \leq 1 \qquad \text{Eq 3.19}$$

Based on Section 3.4.1, the spruce-PUR panel showed the highest stress compared to other studied CLTs. The resulting stresses in the outer layer of selected panels are provided in Table 3.6. σ_L is tensile stresses parallel to the grain (normal stress in *x* direction), σ_{Lc} is compression stresses parallel to the grain (normal compression stress in *x* direction), $\sigma_{R/T}$ is tensile stresses perpendicular to grain (normal stress in *z* direction), $\sigma_{R/Tc}$ is compression stresses perpendicular to grain (normal stress in *z* direction), $\sigma_{LT/LR}$ is longitudinal shear stresses in the LT plane (*xy* component of shear stress), and σ_{RT} is rolling shear stresses (*xz* component of shear stress).

Table 3.6: Obtained stress values for the selected CLT panels.

	$\boldsymbol{\sigma_L}$ (MPa)	$\boldsymbol{\sigma_{Lc}}$ (MPa)	$\boldsymbol{\sigma_{R/T}}$ (MPa)	$\boldsymbol{\sigma_{R/Tc}}$ (MPa)	$\boldsymbol{\sigma_{LT/LR}}$ (MPa)	$\boldsymbol{\sigma_{RT}}$ (MPa)
oak-PVAC	2.9×10^{-7}	-1.5×10^{-7}	3.5×10^{-4}	-1.8×10^{-4}	1.6×10^{-6}	4.58×10^{-7}
pine-PRF	9.2×10^{-3}	-3.8×10^{-3}	1.1×10^{-2}	-4.4×10^{-3}	2.16×10^{-6}	6.13×10^{-7}
pine-PUR	3.6×10^{-3}	-1.5×10^{-3}	4.02×10^{-3}	-6.5×10^{-4}	2.36×10^{-7}	5.93×10^{-7}
spruce-PUR	0.35	-0.35	13.95	-14.865	1.49	1.25

Mechanical properties are measured and represented as strength properties for design in the wood handbook [46]. These strength properties include maximum stress in compression parallel to grain

($f_{c,0}$), compressive stress perpendicular to grain ($f_{c,90}$), shear strength parallel to grain (f_v), tensile strength perpendicular to grain ($f_{t,90}$), tensile strength parallel to grain ($f_{t,0}$), and rolling shear strength (f_{roll}). Table 3.7 gives strength properties of the selected wood species for the studied CLT panels.

Table 3.7: Mechanical properties of the selected materials *[46]*.

species name	Density (kg/m^3)	MC (%)	$f_{c,0}$ (MPa)	$f_{c,90}$ (MPa)	f_v (MPa)	$f_{t,90}$ (MPa)	$f_{t,0}$ (MPa)	f_{roll} (MPa)
oak	717	12	41.8	8.3	12.5	4.7	71	2.25
pin	509	12	47	7	14.3	7.2	97	2.57
spruce	450	12	36	4.3	10.3	1	30	0.5

Failure modes can be determined by replacing simulated stresses according to Table 3.6 and strength properties according to Table 3.7 in failure criteria. The summary of the failure analysis is given in Table 3.8. The result shows that the spruce-PUR panel failed under moisture-induced stress resulting from the 35% humidity difference between exterior and interior surfaces. It is mainly due to the low tensile and compression strengths perpendicular to the grain and the low rolling shear strength of spruce.

Table 3.8: Summary of the failure analysis in the outer layer of selected CLT panels.

	oak-PVAc	**pine-PRF**	**pine-PUR**	**spruce-PUR**	Failure mode	
$F_{t,0}(\sigma) = \frac{\sigma_L}{f_{t,0}} \leq 1$	√	√	√	√	Failure in tension parallel to grain	brittle failure mode
$F_{c,0}(\sigma) = \left\|\frac{\sigma_L}{f_{c,0}}\right\| \leq 1$	√	√	√	√	Failure in compression parallel to grain	ductile failure mode
$F_{t,90R/T}(\sigma) = \frac{\sigma_{R/T}^2}{f_{t,90}^2} + \frac{\sigma_{LT/LR}^2}{f_v^2} + \frac{\sigma_{RT}^2}{f_{roll}^2} \leq 1$	√	√	√	×	Failure in tension perpendicular to grain with splitting in LT and LR plans	brittle failure mode
$F_{c,90R/T}(\sigma) = \left\|\frac{-\sigma_{R/T}}{f_{c,90}}\right\| \leq 1$	√	√	√	×	Failure in pure transverse compression under compression perpendicular to grain	ductile failure mode
$F_{vR/T}(\sigma) = \frac{\sigma_{LT/LR}^2}{f_v^2} + \frac{\sigma_{RT}^2}{f_{roll}^2} \leq 1$	√	√	√	×	Failure in shear under compression perpendicular to grain is distinguished	brittle shear failure

Gereke [27] evaluated the surface quality of the spruce-PUR specimen. The panel was exposed to a 40% humidity difference over 21 days, and the physical evaluation of the panel's bottom layer was reported. Fig 3.16 indicates a brittle failure parallel to the grain due to tension perpendicular to the grain direction on the surface of the bottom layer.

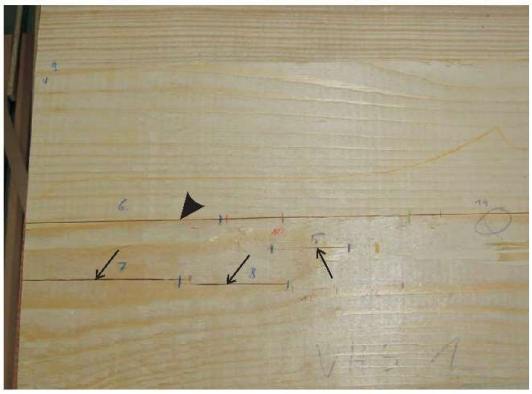

Fig 3.16: Brittle failure on the surface of the outer layer of spruce-PUR panels under a humidity difference of 40% for 21 days *[27]*.

3.4.3 Influence of adhesives' diffusivity on the stress of CLT

This section investigates the influence of adhesives' diffusivity on the moisture-induced stresses of the selected CLT panels. The combination of spruce with three different adhesives (PVAc, PUR, and PRF) was selected. In the first step, the moisture profile of selected panels is simulated according to Section 2.4.2. Then the stresses perpendicular to the grain direction in the middle and outer layers of panels are simulated according to Section 3.4.1. The properties of the spruce and adhesives are given in Table 3.3 and 3.4, respectively. The elasticity of adhesives is assumed constant and equal to 0.36 GPa (equal to the elasticity modulus of PUR) to investigate the effect of adhesives' diffusivity on moisture-induced stress. The result is displayed in Fig 3.17.

Fig 3.17 shows that although the highest adhesive diffusivity (PVAC) resulted in less moisture gradient at the glue line, it leads to higher MC in the middle layer and lower MC in the outer layer of the spruce-PVAc panel. The higher moisture content in the middle layer of spruce-PVAc leads to higher stress perpendicular to the grain direction in the middle layer. Also, lower stress occurs in the outer layer of spruce-PVAc due to less MC in the outer layer. A comparison of spruce-PRF (with the lowest adhesive diffusivity) and spruce-PVAc (with the highest adhesive diffusivity) showed a 19% increase in middle layer stress and a 13% reduction in outer layer stress once adhesivity elasticity increased 30 times.

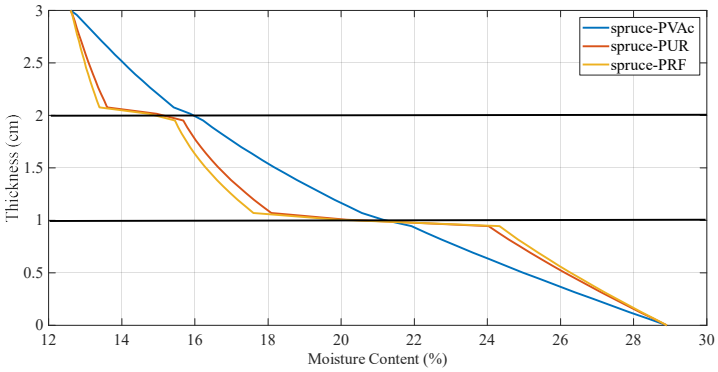

(a)

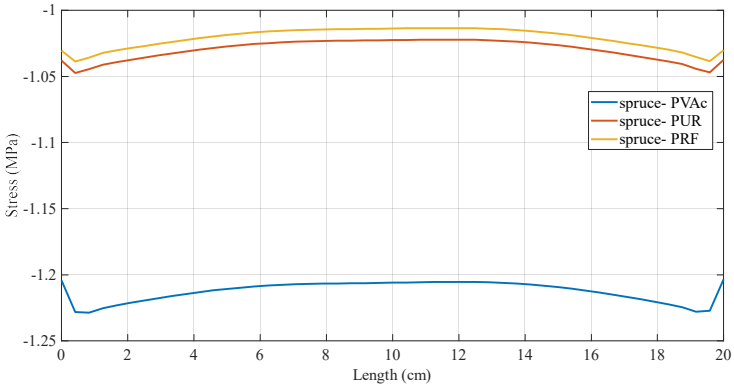

(b)

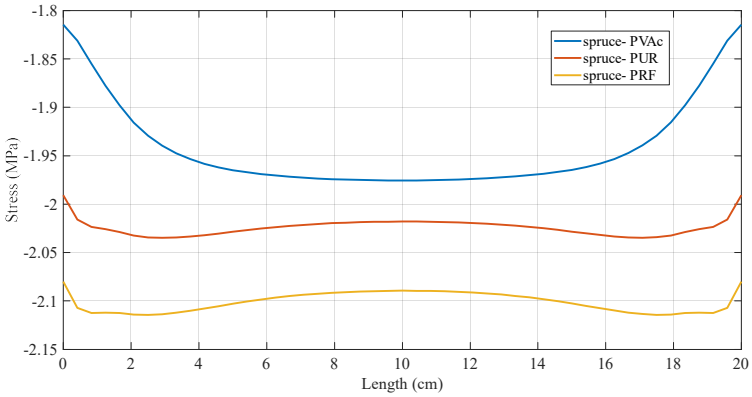

(c)

Fig 3.17: Influence of adhesive's diffusivity on stress, (a) moisture profile, (b) stress perpendicular to grain in the middle layer, (c) stress perpendicular to grain in the outer layer.

3.4.4 Influence of adhesives' elasticity on the stress of CLT

In addition to the diffusion coefficient, adhesive's elasticity affects the moisture-induced stresses in CLT panels. This section investigates the influence of adhesives' elasticity on moisture-induced stress in CLT panels. For this purpose, a constant diffusivity (equal to PUR's diffusivity) is assumed for adhesives. Fig 3.18 displays the simulated moisture profile of selected CLTs. Panel moisture profiles are matched due to the similar diffusivities of adhesives. The obtained stress in the middle and outer layers of selected CLTs is given in Fig 3.18. Comparing spruce-PVAc with spruce-PRF shows that three times decrease in adhesive elasticity resulted in a 70% reduction in stress.

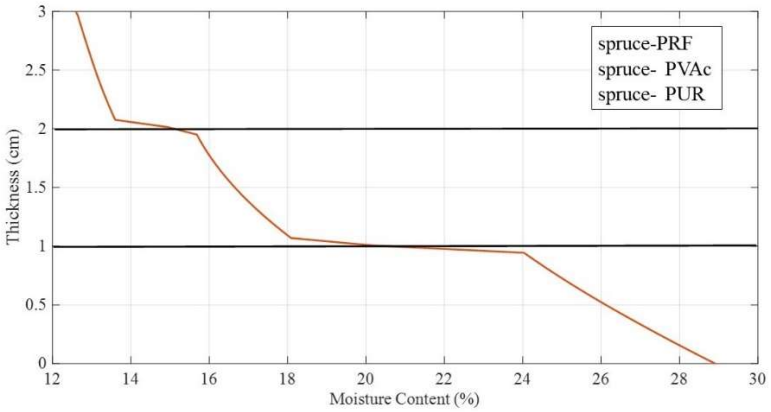

(a)

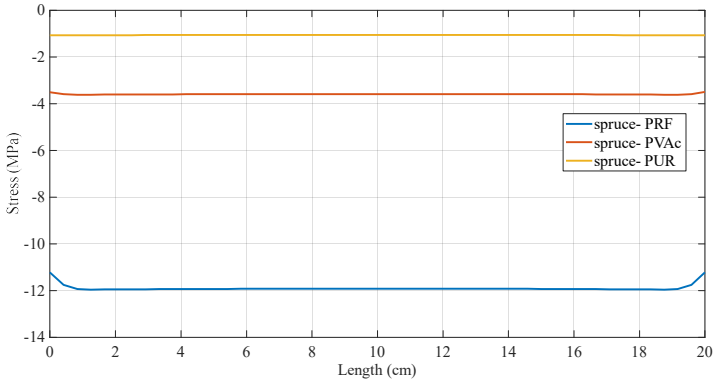

(b)

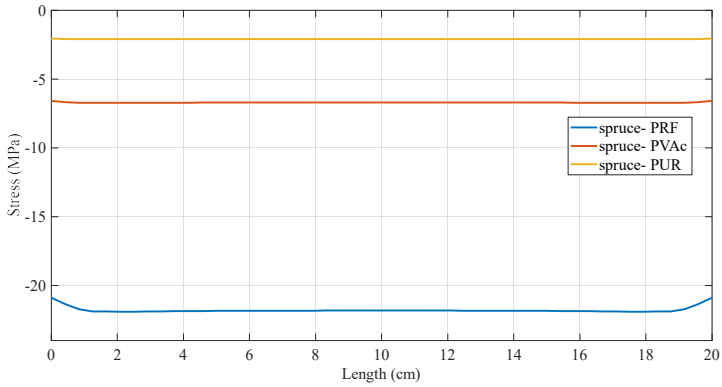

(c)

Fig 3.18: Influence of adhesive's elasticity on stress, a) moisture profile, b) stress perpendicular to grain in the middle layer, c) stress perpendicular to grain in the outer layer.

The same analysis was completed on spruce lumber to compare the stress status of spruce lumber and spruce CLT. Fig 3.19 shows the result of stress perpendicular to grain direction in the middle of the spruce lumber for 14 days of moisture exposure. Spruce CLT experiences a higher compressive stress perpendicular to grain direction, while lumber spruce are under the tensile stress at the middle of the panel thickness. These differences in stress would be occurred due to the higher stress at the place of glues in spruce CLT.

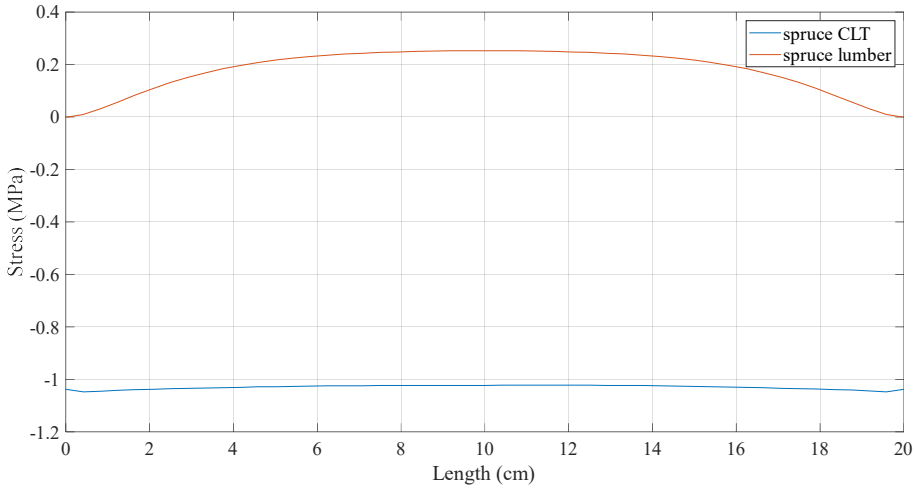

Fig 3.19: Stress perpendicular to the grain in the middle of spruce lumber and spruce CLT

3.5 Conclusion

This chapter presented the numerical modeling of the moisture-induced stresses in CLT panels due to 35% of RH difference for 14 days of moisture exposure. The influences of moisture profiles and adhesive properties on stress results were examined. It was noted that applying porous adhesive in manufacturing CLT panels would reduce the MC gradient and stresses at the glue lines. A higher MC gradient indeed leads to the highest stress in CLT layers. If the strengths of the selected wood for CLT layers were lower than the moisture-induced stress of the wood layer, a crack would develop. The minimum tensile strength of wood perpendicular to its grain direction frequently leads to failure in this direction. The failure analysis showed the spruce-PUR panel was damaged under a 35% humidity difference. This was mainly due to its higher MC and lower perpendicular to grain strength compared to other studied panels.

Applying different CLT adhesives can influence the moisture-induced stress in CLT panels. The moisture-induced stresses could be affected by adhesive diffusivity and adhesive elasticity. Although adhesive diffusivity affects the stress state, their elasticity significantly influences moisture-induced stresses in CLT panels. Using different adhesives yields different moisture contents in CLT's layers, mainly in the middle. Based on the numerical modeling, a rise in the middle layer MC increased stresses perpendicular to the grains in the middle layer. The results also showed that the outer layer was slightly influenced by adhesive diffusivity.

4 Moisture-induced deformation of CLT

4.1 Introduction

Climate gradient leads to considerable deformation in the form of a cup and twist in CLT panels. Moisture-induced deformation reduces the serviceability of the CLT panels. Thus, dimensional stability is of interest for the application of CLT panels. The types of moisture-induced deformation are shown in Fig 4.1. The previous studies showed that the governed moisture-induced deformation in CLT is cup deformation in the *z-y* plane [29]. Hence, the cup deformation of CLT panels is investigated here.

First, previous experimental tests completed by Gereke [29] are presented. Then, numerical modeling of the experiments is discussed. The result of numerical modeling and tests are compared to validate the model. Finally, the model is used for other CLT panels, and the influence of adhesives' properties (diffusion coefficient and elasticity modulus) on the cup deformation of CLTs is investigated.

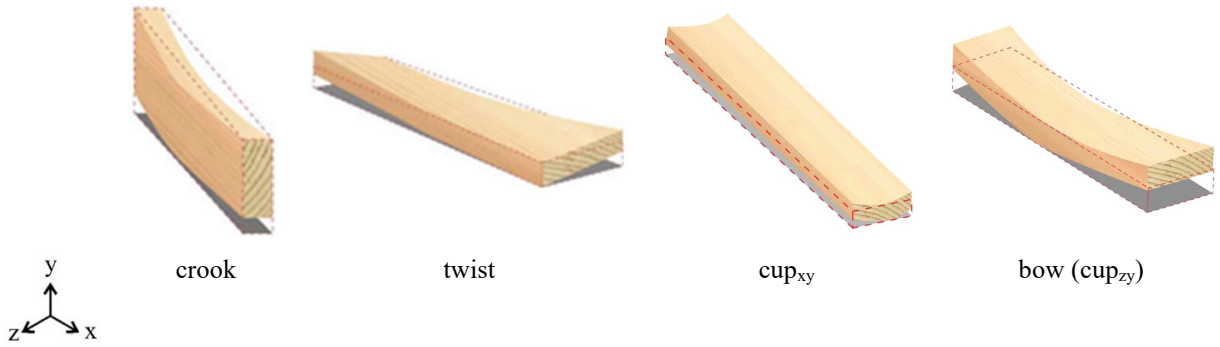

Fig 4.1: The types of moisture-induced deformation in CLT.

4.2 Experiments

A three-layered spruce-PUR panel was tested by Gereke [29] to determine the cup deformation of the CLT panel. The dimension of the panel was $300mm \times 300mm \times 30mm$, and it was initially conditioned at 65% RH. The edge faces of the specimen were sealed to enforce the moisture flow within the panel thickness. Then the panel was placed on three supports, as shown in Fig 4.2. The outer face of the panel was exposed to RH=100% using water in the bottom of the test box.

Displacements in the *y*-direction of the defined points were recorded through dial gauges (Fig 4.2 d) after 14 days of moisture exposure. Based on the displacement of defined points, the cup deformation can be calculated according to Eq 4.1.

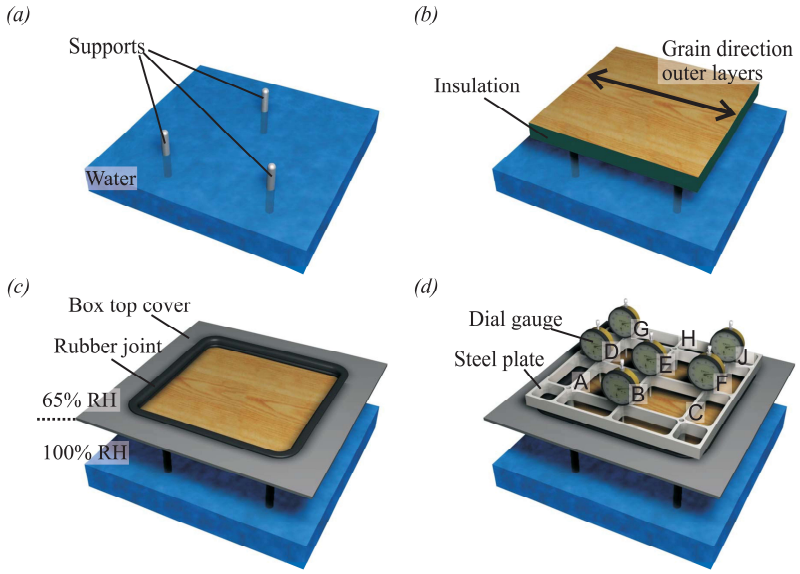

Fig 4.2: Test set-up of the hygroscopic warping experiments *[29]*.

$$cup = \frac{1}{2}\left(\overline{\Delta}_{path\ A} + \overline{\Delta}_{path\ B}\right) + \overline{\Delta}_{path\ C} \qquad \text{Eq 4.1}$$

where $\overline{\Delta}_{path\ A}$ is the average of measured displacement in points A, D, and G, $\overline{\Delta}_{path\ B}$ is the average of measured displacement in points C, F, and J, and $\overline{\Delta}_{path\ C}$ is the average measured displacement in points B, E, and H (see Fig 4.2 d). Under the conditions shown in Fig 4.2, Gereke [29] measured 0.292 *mm* as cup deformation in the *y-z* plane of the spruce CLT panel.

4.3 Numerical modeling

4.3.1 Material

According to the experimental study, spruce and 1K PUR adhesive were used in the modeling. The dependency of the elastic modulus of spruce to moisture content is displayed in Fig 3.5, Fig ***3.6***, and Fig ***3.7*** of Section 3.3.1 and is applied in the model.

Table 4.1 summarizes the required materials' properties according to boundary conditions (RH=65% and RH=100%). Elastic constants of PUR adhesive are 0.36 GPa, 0.18 GPa, and 0.3 as Young's modulus, shear modulus, and Poisson's ratio, respectively [63].

Table 4.1: Summary of Equilibrium Moisture Content (EMC), Moisture Concentration (c), and Moisture Diffusion Coefficient (D) values for spruce and PUR adhesive.

Material	Density (kg/m^3)	EMC (%)	c_{100} (kg/m^3)	c_{65} (kg/m^3)	D (m^2/s)
spruce [27]	450	28.91	130.09	56.7	1.38×10^{-10}
adhesive (PUR) [42]	1000	3.36	33.6	22.2	4.01×10^{-12}

4.3.2 Method

The geometry, boundary condition, and coordinate system are shown in Fig 4.3. The longitudinal axis of these local coordinate systems is aligned parallel to the *x*-axis in the outer layers and parallel to the *z*-axis in the middle layer. Considering 0.1 *mm* thickness for each glue line, the total dimension of the model will be 300*mm*×300*mm*×30.2*mm*. The moisture content applied to the model is simulated based on Section 2.4.2.

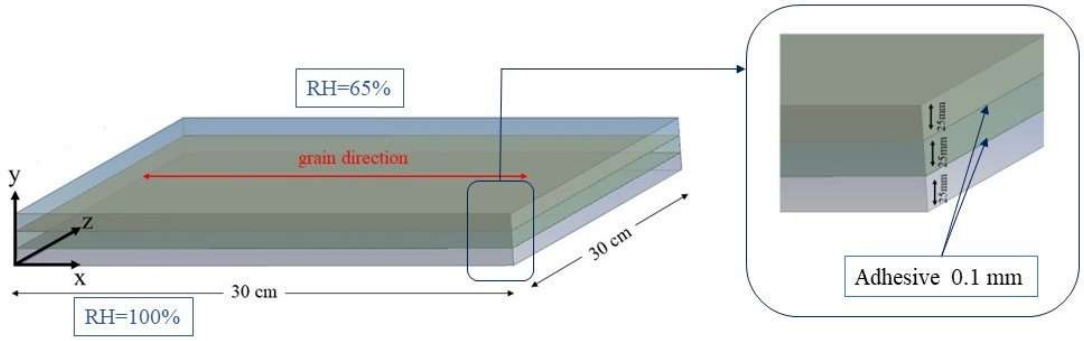

Fig 4.3: Geometry of the model and boundary conditions.

Three paths (A, B, and C) along the *x*-axis are defined at z = 50 *mm*, z = 150*mm*, and z=250*mm* at the bottom of the panel (i.e. y = 0). The average value of y-direction displacement of defined paths is obtained as $\overline{\Delta}_{path\ A}$, $\overline{\Delta}_{path\ B}$, and $\overline{\Delta}_{path\ C}$. Thereupon, the cup deformation can be calculated according to Eq 4.1.

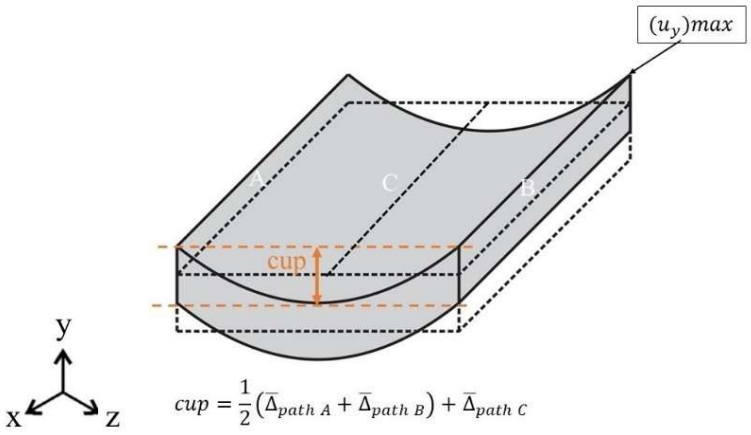

Fig 4.4: cup_{yz} deformation and maximum out of plane deformation of CLT.

4.3.3 Results

The moisture-induced deformation (cup_{yz}) is determined through the defined paths in Fig 4.4. The maximum *y*-direction displacement occurs at the corner of the panel that is reported as $(u_y)_{max}$. The simulated and experiment deformations are given in Table 4.2. Gereke [29] modeled numerically the same experiment, and the result of his modeling was added to the result. Differences between the results would be caused due to the models' assumptions. Gereke [29] applied the varying diffusion coefficient with moisture content for spruce and adhesive based on Eqs 2.3 and 2.4. This study assumed the moisture diffusion of materials is constant. Furthermore, CLT panels are assumed to have the same elastic constants as spruce in numerical simulations (Gereke and this study), despite the fact that the elastic constants are different. This assumption is due to the lack of available experiments measuring the elastic constant of CLT panels.

The same analysis was completed on spruce lumber to compare the deformation status of spruce lumber and spruce CLT. The deformation for the lumber spruce is shown in Table 4,2, as well. result of stress perpendicular to grain direction in the middle of the spruce lumber for 14 days of moisture exposure. Spruce CLT experiences a higher compressive stress perpendicular to grain direction, while lumber spruce are under the tensile stress at the middle of the panel thickness. These differences in stress would be occurred due to the higher stress at the place of glues in spruce CLT.

Table 4.2: Simulated and measured maximum out-of-plane and cup deformation.

This study	Gereke [29]

	Numerical (CLT)	Numerical (Timber)	Numerical (CLT)	Measurement (CLT)
$(u_y)_{max}$ [mm]	0.181		0.196	-
cup_{yz} [mm]	0.204		0.283	0.292

4.4 Parametric studies

The model was validated in Section 4.3.3. Thus, it can be developed to investigate the influence of adhesives' properties on the moisture-induced deformation of different CLT panels. According to Section 3.4, a combination of spruce and three adhesives (PVAc, PUR, and PRF) is selected for completing two case studies. The effect of the adhesive's diffusivity and elasticity on the cup deformation of CLTs are discussed in Sections 4.4.1 and 4.4.2.

4.4.1 Influence of adhesive's diffusivity on moisture-induced deformation of CLT

This section aims to find how adhesives' diffusivity affects the moisture-induced deformation of CLT panels. In the first step, the moisture profile of selected panels is simulated based on Section 2.4.2 as the applied loads. Table 4.3 gives moisture diffusivities of the selected adhesives. Then the cup deformation of panels is simulated according to Section 4.3.2. The elasticity of adhesives is assumed constant and equal to 0.36 GPa (equal to the elasticity modulus of PUR) to investigate the effect of adhesives' diffusivity on moisture-induced deformation. The result is displayed in Fig 4.5.

Table 4.3: Diffusivity of adhesive materials *[42]*.

Material	**D (m^2/s)**
PVAc	17.8×10^{-12}
PUR	4.01×10^{-12}
PRF	0.58×10^{-12}

Fig 4.5 shows the highest MC in the middle layer and lowest MC in the bottom layer of the spruce-PVAc panel compared to other panels. It occurs due to the highest moisture diffusivity of PVAc adhesive. Comparing the deformation result of spruce-PRF (with the lowest adhesive diffusivity)

to spruce-PVAc (with the highest adhesive diffusivity) showed that 30 times increase in adhesive moisture diffusivity leads to a 10% decrease in the cup deformation.

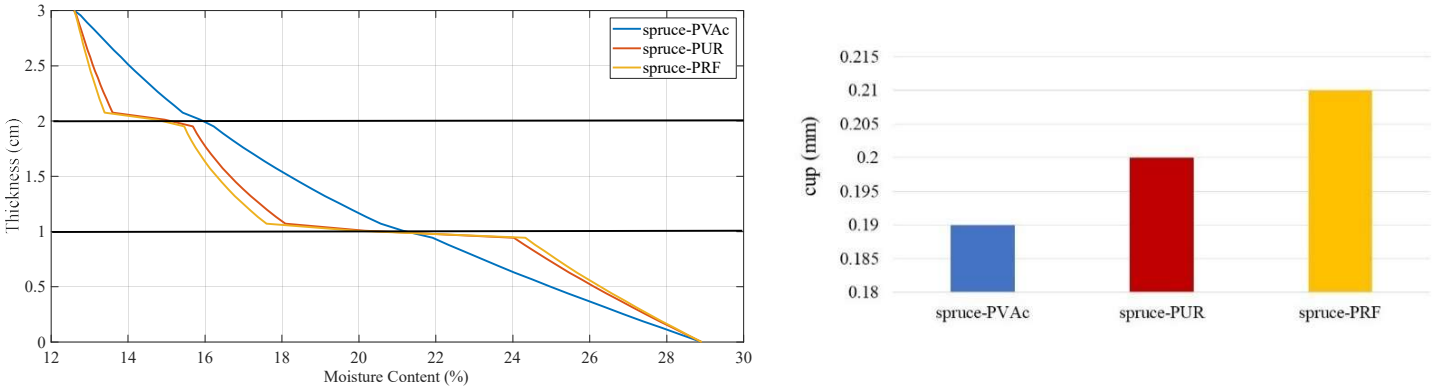

(a) (b)

Fig 4.5: Influence of adhesive's diffusivity on moisture-induced deformation of CLT, (a) moisture profile, (b) cup deformation.

4.4.2 Influence of adhesive's elasticity on moisture-induced deformation of CLT

This section investigates the influence of adhesive elasticity on moisture-induced deformation in CLT panels. For this purpose, a constant moisture diffusivity (equal to PUR diffusivity) is assumed for adhesives. The elastic constant of the selected adhesives is listed in Table 4.4. PRF and PUR have the highest and lowest elasticity, respectively.

Table 4.4: Modulus elasticity of adhesive materials *[63]*.

Material	E (GPa)
PUR	0.36
PVAc	1.1
PRF	3.5

Fig 4.6 displays the simulated moisture profile and cup deformation of selected CLT panels. A comparison of spruce-PUR and spruce-PRF revealed that a ten-fold increase in adhesive elasticity leads to a 5% reduction in panel cup deformation.

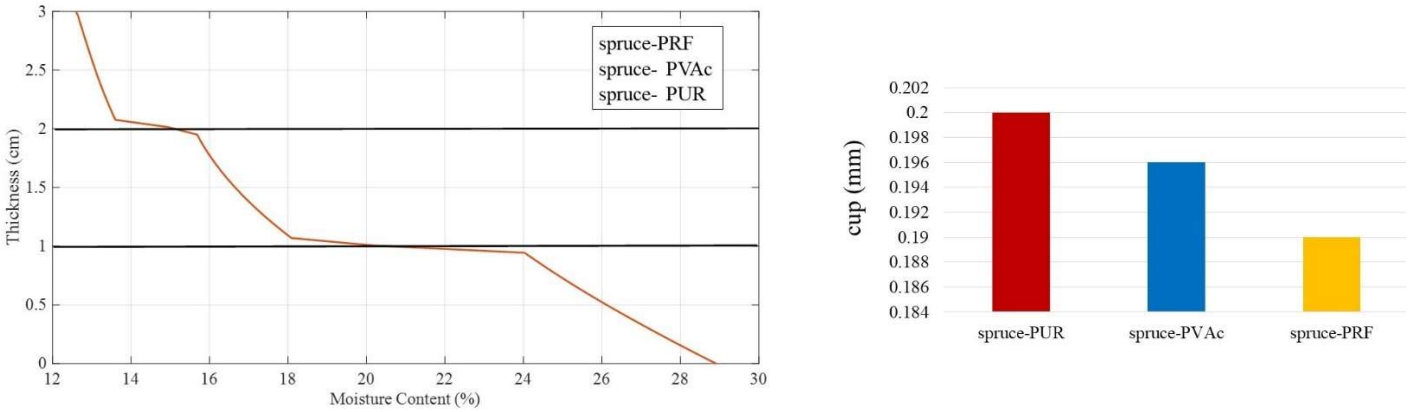

(a) (b)

Fig 4.6: Influence of adhesive's elasticity on moisture-induced deformation of CLT, (a) moisture profile, (b) cup deformation.

4.5 Conclusion

This chapter investigated moisture-induced deformation in CLT panels. A 65-100% RH induced the cup deformation in selected panels. Previous studies have shown that the main form of deformation occurs in the *y-z* plane as cup_{yz}. The measured deformations in the literature were used to validate the numerical model. Then the model was developed for further parametric studies. The parametric studies were completed to investigate the influence of adhesives properties (moisture diffusivity and elasticity) on the moisture-induced deformation of CLT panels.

The coefficient of moisture diffusion of the glue lines was found to significantly influence the cup deformation of the CLT panels. With increased moisture diffusivity of the adhesive, deformation was reduced. Thus, using adhesives with low moisture resistances (i.e. high moisture diffusivity) in CLTs would help to avoid panel deforming due to moisture variations across the panel thickness. Additionally, the effect of glue line stiffness on moisture-induced deformation of CLTs was studied by applying three adhesives with different elasticities. The result indicated employing an adhesive with higher elasticity in CLT manufacturing could result in a lower moisture-induced deformation of CLT panels.

5 Summary and conclusion

Cross Laminated timber panels may be exposed to cyclic environmental conditions that would result in cracks or deforming the panels due to moisture-induced stresses and deformations. These

stresses and deformations would reduce the strength and serviceability of CLT panels, affecting their applications. These stresses and deformations were investigated based on numerical simulations, considering adhesive effects. In this research, moisture differences between panel surfaces were considered as a moistening scenario.

Predicting the moisture profile variation over time (for various moistening scenarios) was the first step toward understanding the performance of laminated products under environmental loads. Previous experimental tests on measuring moisture content, moisture-induced stresses, and deformations were used in this study for model validation purposes. Then the model was developed for other CLTs to investigate the influence of various parameters on moisture profile, moisture-induced stress, and deformations.

The moisture content in CLT layers caused by a change in the humidity of ambient air depends on parameters such as the moisture diffusion coefficient of adhesive and wood species, the middle layer material, moisture exposure time duration, and layers arrangement.

The measured moisture content of the CLT panel indicated that glue lines provide high moisture resistance. Previous numerical studies also showed that the selected values for the moisture diffusion coefficient of materials could significantly affect the moisture transfer across the multi-layered composite panels. However, these models were only valid for the selected materials (spruce and 1K PUR) and could not be developed for other CLTs made of different materials. This study introduces a framework to predict the moisture profile of all multi-layered composite panels glued with different adhesives. Also, unlike previous studies, instead of employing the surface emission coefficient, the moisture adsorption curve of the material was used as an alternative but simple approach to estimate moisture flux at the surfaces.

Although the previous studies showed that moisture diffusivity varies with the material's moisture content, this study demonstrated that such variation might not significantly affect the CLT panels' moisture profile. This is due to the generated moisture gradient at the glue lines. Such gradient was shown to be different in various composites and depended on the value of D_{adh}. When D_{adh} was smaller than the layers' D, the moisture gradient across the panel thickness was significant. This matter led to large moisture gradients between layers. When D_{adh} was close to the main layers' D, the moisture gradient was found to be negligible, and a more uniform moisture profile was achieved. It could be concluded that, depending on the selected wood species, the proper choice

of adhesive for manufacturing laminated panels can affect the moisture gradient across the glue lines later in the product's service life.

Using a different material for the middle layer led to very distinct profiles, especially in the middle of the panels. Results demonstrated that using a material with higher diffusivity for the middle layer of the CLT panel can lead to a higher moisture content in this layer compared to face layers. The very high moisture gradient found across the glue lines suggests that different species should be mixed with care in manufacturing laminated panels.

Adhesive types did not affect the short-term moisture profile of CLT panels even when exposed to high humidity differences between the panel surfaces. Because, in the short-term time duration (1 hour), there was not enough time to let moisture reaches the glue line. As a result, the short-term moisture profiles of CLT panels glued with various adhesive types were the same. Hence, the long-term performance of CLT panels should be considered in designing CLT panels.

Using orthotropic moisture diffusivity resulted in a more realistic moisture content in CLT layers. However, the difference in moisture profile was not significant (4%). Therefore, considering moisture diffusivity in all directions equal to D_T is an acceptable assumption in the moisture transport simulations. When the boundary conditions of the panel surfaces are altered, layer arrangements of CLT panels must be considered in determining their moisture profile.

Moisture-induced stresses and deformations in CLT panels depend on various parameters. The literature has shown the influence of wood species, layer thickness ratio, annual ring direction of wood species, and prestressed wood species on the moisture-induced stress state in CLT panels. This study investigated the influence of other parameters, adhesive diffusivity, and modulus of elasticity, on stresses and deformations of CLT panels caused by changing ambient air humidity.

The moisture profile of the panel influences stresses and deformations induced by both a moisture gradient and climate change. With an increased moisture content of the layers, the moisture-induced stresses increased. The higher moisture gradient at the glue lines leads to the greatest stresses at glue lines. Application of different adhesive types would lead to different scenarios in the moisture content of CLT layers. Higher diffusivity of the adhesive leads to a lower moisture gradient at the place of glue lines, which results in minor stress at bonding lines. Also, a lower moisture gradient is expected for the bottom layer when a more porous adhesive is used in CLT

panels. On the other hand, using an adhesive with lower resistance to moisture transfer resulted in higher moisture content in the middle layer, consequently causing higher stress in the middle layer.

The stiffness of glue lines showed a significant influence on stresses. A three-fold decrease in adhesive elasticity resulted in a 70% reduction in stresses. Therefore, it can be concluded that using an adhesive with higher diffusivity and lower elasticity would result in lower stresses.

The moisture-induced deformation of CLT panels was reduced when an adhesive with higher diffusivity was applied to bonding CLT layers. The adhesive elasticity has a negligible impact on CLT deformation. The deformation of the adhesive was reduced by 5% when the adhesive elasticity was ten times lower. It is concluded that while adhesive elasticity has very little influence on deformation, diffusivity was found to influence both stress and deformation. Thus, stresses and deformations could be minimized with the correct choice of adhesive (higher diffusivity and lower elasticity) for the static requirements and the expected climatic conditions.

The result of this study showed how moisture variations could affect the long-term performance of sustainable composite panels made from natural resources and various adhesives. As demonstrated in the parametric studies, the model can be used as a tool to guide panel manufacturers to design durable products with optimized adhesive characteristics engineered for different climate conditions to reduce moisture-induced stresses and deformations.

5.1 Future work

Although the developed model in this study was quite comprehensive, there were some research limitations due to assumptions made and the lack of accurate experimental data. Such limitations can be addressed in future studies. Static and dynamic loads were excluded from the investigations of the present thesis. Understanding the performance of CLT panels under combined mechanical and environmental loads is required to extend the knowledge about the physical behavior of laminated panels.

The temperature is assumed to be constant in this study. The influences of temperature on moisture diffusion coefficient, equilibrium moisture content, moisture uptake curves, and elastic constants of materials were neglected. However, these parameters would be affected by temperature. While higher temperature would result in higher moisture diffusivity, it causes lower values for

equilibrium moisture content, moisture uptake curves, and elastic constants of materials. Thus, a combined heat and moisture transport model can be considered in future work in this area.

This study has not examined a complete structure of a large CLT panel with several wooden planks in each layer. The significant role of connection materials (adhesives) on moisture transport, moisture-induced stresses, and deformations was shown. So, based on the manufacturing process, studying the effect of planks' connection type on moisture-induced stresses and panel deformations is strongly recommended for future work.

References

[1] X. Sun, M. He, and Z. Li, "Novel engineered wood and bamboo composites for structural applications: State-of-art of manufacturing technology and mechanical performance evaluation," *Construction and Building Materials*, vol. 249, p. 118751, 2020.

[2] S. J. Pang and G. Y. Jeong, "Swelling and shrinkage behaviors of cross-laminated timber made of different species with various lamina thickness and combinations," *Construction and Building Materials*, vol. 240, Apr. 2020, doi: 10.1016/j.conbuildmat.2019.117924.

[3] Structurlam, "Structural Mass Timber Technical Guide for CrossLam® CLT and GlulamPLUS®." 2022.

[4] S. Florisson, "Moisture-induced stress and distortion of wood: A numerical and experimental study of wood's drying and long-term behaviour," PhD Thesis, Linnaeus University Press, 2021.

[5] C. Bylund Melin, C.-E. Hagentoft, K. Holl, V. M. Nik, and R. Kilian, "Simulations of moisture gradients in wood subjected to changes in relative humidity and temperature due to climate change," *Geosciences*, vol. 8, no. 10, p. 378, 2018.

[6] J. Tripathi and R. W. Rice, "Finite Element Modelling of Heat and Moisture Transfer through Cross Laminated Timber Panels," *BioResources*, vol. 14, no. 3, pp. 6278–6293, 2019.

[7] P. Dietsch, A. Gamper, M. Merk, and S. Winter, "Monitoring building climate and timber moisture gradient in large-span timber structures," *Journal of Civil Structural Health Monitoring*, vol. 5, no. 2, pp. 153–165, 2015.

[8] W. T. Simpson, "Predicting equilibrium moisture content of wood by mathematical models," *Wood and fiber science*, vol. 5, no. 1, pp. 41–49, 1973.

[9] R. C. Weatherwax and A. J. Stamm, "The coefficients of thermal expansion of wood and wood products," *Forest Products Laboratory,United States Department of Agriculture Forest Service*, 1956.

[10] A. J. Hailwood and S. Horrobin, "Absorption of water by polymers: analysis in terms of a simple model," *Transactions of the Faraday Society*, 1946.

[11] B. Franke and S. Franke, "Moisture diffusion in wood–Experimental and numerical investigations," *World Conference on Timber Engineering*, 2016.

[12] S. Svensson, G. Turk, and T. Hozjan, "Predicting moisture state of timber members in a continuously varying climate," *Engineering Structures*, vol. 33, pp. 3064–3070, 2011.

[13] S. Fortino and A. Genoese, "Numerical modelling of the hygro-thermal response of timber bridges during their service life: a monitoring case-study," *Construction and Building Materials*, vol. 47, 2013.

[14] M. Autengruber and M. Lukacevic, "Finite-element-based prediction of moisture-induced crack patterns for cross sections of solid wood and glued laminated timber exposed to a realistic climate," *Construction and Building Materials*, vol. 271, p. 27, 2021.

[15] A. Bayatkashkoli and M. Faegh, "Evaluation of mechanical properties of laminated strand lumber and oriented strand lumber made from Poplar wood (Populus deltoides) and Paulownia (Paulownia fortunei) with urea formaldehyde adhesive containing nanoclay," *International Wood Products Journal*, vol. 5, no. 4, pp. 192–195, Nov. 2014, doi: 10.1179/2042645314Y.0000000064.

[16] Z. Wang, M. Gong, and Y. Chui, "Mechanical properties of laminated strand lumber and hybrid cross-laminated timber," *Construction and Building Materials*, vol. 101, pp. 622–627, Dec. 2015, doi: 10.1016/j.conbuildmat.2015.10.035.

[17] J. Tripathi and R. Rice, "Thermal conductivity values for laminated strand lumber and spruce for use in hybrid cross-laminated timber panels," *BioResources*, vol. 12, no. 4, pp. 8827–8837, 2017.

[18] V. Samuel Glass, "Hygrothermal Anaylsis of Wood-Frame Wall Assemblies in a Mixed-Humid Climate," *Forest Products Laboratory*, 2013.

[19] A. A. Chiniforush, H. Valipour, and A. Akbarnezhad, "Water vapor diffusivity of engineered wood: Effect of temperature and moisture content," *Construction and Building Materials*, vol. 224, pp. 1040–1055, Nov. 2019, doi: 10.1016/j.conbuildmat.2019.08.013.

[20] S. Aicher and H.-W. Reinhardt, "Delamination properties and shear strength of glued beech wood laminations with red heartwood," *European Journal of Wood and Wood Products*, vol. 65, pp. 125–136, Jan. 2007.

[21] P. Maimí, P. P. Camanho, J. A. Mayugo, and C. G. Dávila, "A continuum damage model for composite laminates: Part I–Constitutive model," *Mechanics of materials*, vol. 39, no. 10, pp. 897–908, 2007.

[22] H. Bader, P. Niemz, and W. Sonderegger, "Investigation on the influence of the panel composition on selected properties of three-layer solid wood panels," *Holz als roh-und werkstoff*, vol. 65, no. 3, pp. 173–181, 2007.

[23] A. A. Chiniforush, A. Akbarnezhad, H. Valipour, and S. Malekmohammadi, "Moisture and temperature induced swelling/shrinkage of softwood and hardwood glulam and LVL: An experimental study," *Construction and Building Materials*, vol. 207, pp. 70–83, 2019.

[24] M. Ekevad and A. Axelsson, "Variation of modulus of elasticity in the tangential direction with moisture content and temperature for Norway spruce (Picea abies)," *BioResources*, vol. 7, no. 4, pp. 4730–4743, 2012.

[25] R. Popper, P. Niemz, and G. Eberle, "Equilibrium moisture content and swelling of the solid wood panels," *Holz als Roh-und Werkstoff*, vol. 62, no. 3, pp. 209–217, 2004.

[26] P. Niemz, H. Petzold, and P. Haupl, "Measurement and simulation of the moisture content changes in three-layer solid wood panels at different climates," *Holz als Roh-und Werkstoff*, vol. 61, no. 1, pp. 8–12, 2003.

[27] T. Gereke, "Moisture-induced stresses in cross-laminated wood panels," ETH Zurich, 2009.

[28] T. Gereke and P. Niemz, "Moisture-induced stresses in spruce cross-laminates," *Engineering Structures*, vol. 32, no. 2, pp. 600–606, 2010.

[29] T. Gereke, P. J. Gustafsson, K. Persson, and P. Niemz, "Experimental and numerical determination of the hygroscopic warping of cross-laminated solid wood panels," 2009.

[30] C. Bylund Melin, C.-E. Hagentoft, K. Holl, V. M. Nik, and R. Kilian, "Simulations of moisture gradients in wood subjected to changes in relative humidity and temperature due to climate change," *Geosciences*, vol. 8, no. 10, p. 378, 2018.

[31] J. Tripathi and R. W. Rice, "Finite Element Modelling of Heat and Moisture Transfer through Cross Laminated Timber Panels," *BioResources*, vol. 14, no. 3, pp. 6278–6293, 2019.

[32] J. F. Siau, *Transport processes in wood*, vol. 2. Springer Science & Business Media, 2012.

[33] P. K. Kushwaha and R. Kumar, “Studies on water absorption of bamboo-polyester composites: effect of silane treatment of mercerized bamboo,” *Polymer-Plastics Technology and Engineering*, vol. 49, no. 1, pp. 45–52, 2009.

[34] J. A. Stahlhut, “Effect of Absorption of Liquids on the Mechanical Properties of Balsa Wood,” *The UNSW Canberra at ADFA Journal of Undergraduate Engineering Research*, vol. 6, no. 1, 2014.

[35] V. Legrand, L. TranVan, F. Jacquemin, and P. Casari, “Moisture-uptake induced internal stresses in balsa core sandwich composite plate: Modeling and experimental,” *Composite Structures*, vol. 119, pp. 355–364, 2015.

[36] F. Liu, G. Han, W. Cheng, and Q. Wu, “Sorption isotherm of southern yellow pine high density polyethylene composites,” *Materials*, vol. 8, no. 1, pp. 368–378, 2015.

[37] P. N. Peralta and A. W. C. Lee, “Unsteady-state diffusion of moisture in giant timber bamboo (Phyllostachys bambusoides Sieb. \& Zucc.),” *Wood and fiber science*, vol. 27, no. 4, pp. 421–427, 1995.

[38] Z. Perkowski, J. Świrska-Perkowska, and M. Gajda, “Comparison of moisture diffusion coefficients for pine, oak and linden wood,” *Journal of building physics*, vol. 41, no. 2, pp. 135–161, 2017.

[39] M. Borrega and L. J. Gibson, “Mechanics of balsa (Ochroma pyramidale) wood,” *Mechanics of Materials*, vol. 84, pp. 75–90, 2015.

[40] DIN, “Testing of wood; determination of moisture content (DIN 52183),” vol. 11, 1977.

[41] J. F. Siau, *Wood: Influence of moisture on physical properties*. Department of Wood Science and Forest Products, Virginia Polytechnic, 1995.

[42] R. Wimmer, O. Kläusler, and P. Niemz, “Water sorption mechanisms of commercial wood adhesive films,” *Wood science and technology*, vol. 47, no. 4, pp. 763–775, 2013.

[43] S. Avramidis, “Bound water migration in wood,” *Fundamentals of wood drying*, pp. 105–124, 2007.

[44] American Society of Heating, Refrigeration and Air-Conditioning Engineers., *ASHRAE handbook: Fundamentals*. 2009.

[45] C. Skaar, “Electrical Properties of Wood,” pp. 207–262, 1988, doi: 10.1007/978-3-642-73683-4_6.

[46] R. J. Ross -, “Wood handbook: wood as an engineering material,” *Forest Products Laboratory,United States Department of Agriculture Forest Service*, 2010.

[47] W. U. Sonderegger, “Experimental and theoretical investigations on the heat and water transport in wood and wood-based materials,” 2011, doi: 10.3929/ethz-a-006532317.

[48] S. Srpčič, J. Srpčič, M. Saje, and G. Turk, “Mechanical analysis of glulam beams exposed to changing humidity,” *Wood Science and Technology*, vol. 43, no. 1, pp. 9–22, 2009.

[49] E. C. F. ISO, “Hygrothermal performance of building materials and products (ISO 12572),” *Determination of water vapour transmission properties-Cup Method, Brussels*, vol. 36, 2016.

[50] J. Crank, *The mathematics of diffusion*. Oxford university press, 1979.

[51] J. F. Siau and S. Avramidis, “The surface emission coefficient of wood,” *Wood and Fiber Science*, vol. 28, no. 2, pp. 178–185, 1996.

[52] D. Honfi, A. Mårtensson, S. Thelandersson, and R. Kliger, “Modelling of bending creep of low-and high-temperature-dried spruce timber,” *Wood science and technology*, vol. 48, no. 1, pp. 23–36, 2014.

[53] J. Eitelberger and K. Hofstetter, “A multi-scale approach for simulation of transient moisture transport processes in wood below the fiber saturation point,” *Composites Science and Technology*, vol. 71, pp. 1727–1738, 2011.

[54] J. Y. Liu and W. T. Simpson, “Solutions of diffusion equation with constant diffusion and surface emission coefficients,” *Drying Technology*, vol. 15, no. 10, pp. 2459–2477, 1997.

[55] S. Ormarsson, “Numerical analysis of moisture-related distortion in sawn timber,” PhD Thesis, Chalmers University of Technology, Dep. of Structural Mech, 1999.

[56] Z. Afshari and S. Malek, “Moisture transport in laminated wood and bamboo composites bonded with thin adhesive layers–A numerical study,” *Construction and Building Materials*, vol. 340, p. 127597, 2022.

[57] J. Fourier, “Analytical Theory of Heat, Translated with notes of A,” *FREE-MAN, New York*, vol. 359, 1955.

[58] S. Yoon, B. Han, and Z. Wang, “On moisture diffusion modeling using thermal-moisture analogy,” 2007.

[59] D. Konopka, “Transient multi-Fickian hygro-mechanical analysis of wood,” *Computers & Structures*, vol. 197, pp. 12–27, 2018.

[60] T. Zhan *et al.*, “Moisture diffusion properties of graded hierarchical structure of bamboo: longitudinal and radial variations,” *Construction and Building Materials*, vol. 259, p. 119641, 2020.

[61] M. Kadivar, C. Gauss, K. Ghavami, and H. Savastano, “Densification of Bamboo: State of the Art,” *Materials*, vol. 13, no. 19, p. 4346, 2020.

[62] A. Rosenkilde, “Moisture content profiles and surface phenomena during drying of wood,” PhD Thesis, Byggvetenskap, 2002.

[63] J. Konnerth, W. Gindl, and U. Müller, “Elastic properties of adhesive polymers. I. Polymer films by means of electronic speckle pattern interferometry,” *Journal of applied polymer science*, vol. 103, no. 6, pp. 3936–3939, 2007.

[64] O. Dahlblom, S. Ormarsson, and H. Petersson, “Simulation of wood deformation processes in drying and other types of environmental loading,” in *Annales des sciences forestieres*, 1996, vol. 53, no. 4, pp. 857–866.

[65] A. Ranta-Maunus, “Impact of mechano-sorptive creep to the long-term strength of timber,” *Holz als Roh-und Werkstoff*, vol. 48, no. 2, pp. 67–71, 1990.

[66] E. GÜNTEKİN, T. Y. AYDIN, and P. NİEMZ, “Some orthotropic mechanical properties of Sessile oak (Quercus petrea) as influenced by moisture content,” *Eurasian Journal of Forest Science*, vol. 4, no. 1, pp. 40–47, 2016.

[67] M. Autengruber, M. Lukacevic, and J. Füssl, “Finite-element-based moisture transport model for wood including free water above the fiber saturation point,” *International Journal of Heat and Mass Transfer*, vol. 161, p. 120228, Nov. 2020.

[68] S. Holmberga, K. Perssona, and H. Peterssonb, “Nonlinear mechanical behaviour and analysis of wood and fiber materials,” *Computers & Structures*, vol. 72, no. 4–5, pp. 459–480, 1999.

[69] C. Sandhaas, J.-W. Van de Kuilen, and H. J. Blass, “Constitutive model for wood based on continuum damage mechanics,” in *WCTE, World conference on timber engineering, Auckland, New Zealand, 15-19 July 2012*, 2012.

[70] S. W. Tsai and E. M. Wu, “A general theory of strength for anisotropic materials,” *Journal of composite materials*, vol. 5, no. 1, pp. 58–80, 1971.